Title	部位特異的RNA編集を用いたインビトロでの青色蛍光タンパク質（BFP）から緑色蛍光タンパク質（GFP）への変換に関する研究
Author(s)	Vu, Thi Luyen
Citation	
Issue Date	2015-09
Type	Thesis or Dissertation
Text version	ETD
URL	http://hdl.handle.net/10119/12982
Rights	
Description	Supervisor:塚原　俊文，マテリアルサイエンス研究科，博士

JAIST
JAPAN
ADVANCED INSTITUTE OF
SCIENCE AND TECHNOLOGY

Study on Conversion from Blue Fluorescent Protein (BFP) to Green Fluorescent Protein (GFP) *in vitro* by Using Site-Directed Chemical RNA Editing

VU THI LUYEN

Japan Advanced Institute of Science and Technology

Doctoral Dissertation

Study on Conversion from Blue Fluorescent Protein (BFP) to Green Fluorescent Protein (GFP) *in vitro* by Using Site-Directed Chemical RNA Editing

VU THI LUYEN

Supervisor: Professor Dr. Toshifumi Tsukahara

School of Materials Science

Japan Advanced Institute of Science and Technology

September 2015

Doctoral Dissertation

Study on Conversion from Blue Fluorescent Protein (BFP) to Green Fluorescent Protein (GFP) *in vitro* by Using Site-Directed Chemical RNA editing

Main theme advisor Professor Dr. Toshifumi Tsukahara

Sub theme advisor Associate Professor Dr. Dam Hieu Chi

Judging Committee

Head of Committee Professor Dr. Toshifumi Tsukahara

Internal Committee Professor Dr. Shin-ya Ohki

Internal Committee Professor Dr. Takahiro Hohsaka

Internal Committee Associate Professor Dr. Hidekazu Tsutsui

External Committee Dr. Shinichi Takeda

School of Materials Science

Japan Advanced Institute of Science and Technology

VU THI LUYEN

s1040201

ABSTRACT

RNA editing is the post-transcriptional process to modify the sequence of RNA. This process generated the diversity of RNA and various functions of protein. Abnormal RNA editing can cause many human diseases and pathophysiology such as neurological disorders and cancers. In human, A-to-I editing and C-to-U editing are two popular types of RNA editing. Because the RNA editing is power to recode genetic information of RNA, there are many efforts to control or mimic RNA editing.

C-to-U editing has very promising application for treatment of diseases which were caused by T>C or G>A mutations. We recently reported a strategy for site-directed, non-enzymatic, chemical RNA editing that allows application of C-to-U editing. By reprogramming guanosine to adenosine, this method has great potential to partly repair genetic disease phenotypes. Our method is simple, not expensive and non-toxic because the recombinant enzyme was not used. Our strategy was firstly reported by Prof. Fujimoto and colleagues. In their protocol, template-directed DNA photoligation was mediated by artificial oligonucleotides. A short 20-mer target was used, and C-to-U substitution was efficient, sequence-specific without any side-reactions *in vitro*. In our work, we studied and developed this method to apply for long DNA and full-length RNA targets.

In our overall phototherapy strategy, ultra-violet A (366nm UV) was used to generate the photo-crosslinking between the 5'- carboxyvinyldeoxyuridine nucleoside- (^{CV}U) ODNs with targeted cytosine on RNA. And we could carry out the deamination reaction by heat-treatment through the interaction. Finally, the cross-linked nucleotide was cleaved by the photospliting operation (UVB radiation; 312nm). UVB phototherapy was used as common treatment modality for psoriasis and other skin diseases. Although UVB related to the skin carcinogenesis, until now all reports showed that UVB phototherapy generally did not increase the skin cancer risk. Therefore, UVB phototherapy was evaluated a very safe treatment modality.

To investigate the photochemical editing, we used a mitochondrial DNA T8993C mutation of Leigh syndrome patient as first model. Leigh syndrome is a devastating, neurodegenerative disorder. Leigh syndrome is estimated about 1 of 40,000 live births, and this disease has related to the transversion 8993T>G of ATPase6 gene in mitochondrial DNA. The gene ATPase6 encodes for a subunit of respiratory-chain complex V. The results were revealed that we succeeded a sequence-specific photochemical base substitution toward various targets including synthetic single strand 72 nucleotide (ss72-nt), ss731-nt, RNA 823-nt, and total RNA from patient's cells. We determined that approximately 10% of the full-length mRNA was targeted in *in vitro* deamination under physiological temperature.

The Leigh syndrome patient's cells slowly grow, and these cells are very difficult to absorb the exogenous ODNs, therefore, we used blue fluorescent protein-BFP, a derivate of green fluorescent protein-GFP as new, suitable model. The PCR-RFLP and spectrofluorometric results showed that site-directed photochemical base substitution was successfully performed in synthetic ss100-nt and *in vitro*-synthesized full-length BFP mRNA targets. Among the three tested ^{CV}U-containing ODNs, ODNc exhibited approximately 10% efficiency for C199U transition under physiological temperature. The efficiency was not so high, but this is a first step toward using non-enzymatic, site-directed transition for restoring mutated mRNAs.

The structure and sequence of ^{CV}U-containing ODNs are key features of ODNs on its biological functions. To investigate the relationship between the ^{CV}U sequences and deamination efficiency a series of oligodeoxynucleotides (ODNs) were subjected to site-directed, non-enzymatic editing. By also using a transition from cytosine (C) of blue fluorescent protein (BFP) gene to uridine (U) of green fluorescent protein (GFP) gene at position 199 as a model, the experimental results revealed that the structural sequence dependent deamination efficiency was very tight *in vitro*. The optimum length of hairpin was 8nt and the optimum length of complementary sequence was from 15-17nt. The deamination efficiency of ODN8 was 12% for C199U transition under physiological temperature. This study has important significance to design the suitable, optimum ODNs for treatment of every T>C or G>A caused diseases.

Key words: Chemical RNA editing, photochemical reaction, deamination, antisense oligodeoxyribonucleotide, ^{CV}U oligodeoxynucleotide

CONTENTS

CHAPTER-1: GENERAL INTRODUCTION

1.1. Gene mutations and the genetic diseases caused by C-T and G-A point mutations

Gene is one basic physical and functional unit of inheritance [1]. Gene is composed by DNA and the building blocks of DNA are nucleotides. There are four types of nucleotides. All nucleotides contain phosphate, sugar, and one of four bases nucleotide which are adenine, guanine, cytosine, and thymine. Four base nucleotides are divided into two groups. The first one is purines including adenine and guanine and the second one is pyrimidines containing cytosine and thymine (Fig.1.1) [2].

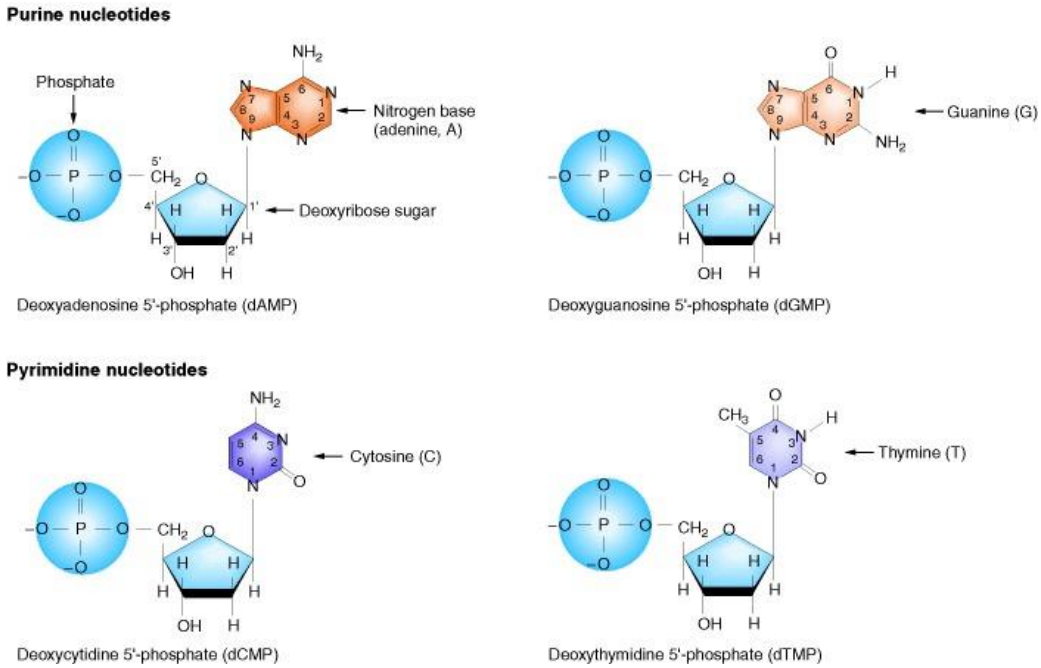

Figure 1.1: Chemical structures of four nucleotides [2]

The nucleotide sequences of genes and the live information usually are preservation from the generations. However, the spontaneous errors in DNA replication or induced errors from the damaging effects of mutagens (such as chemicals or radiations) are the causes of the gene mutations [3]. Therefore, the gene mutations are defined as changes of nucleotide sequences of gene. Because such the changes are taken place in one gene, gene mutation is sometimes called the point mutation [4]. Mutation rater at the base mutation in humans was measurement and estimated within the range 2.5×10^{-9} to 9.0×10^{-8} per base pair per generation [5-7].

There are two types of point mutations which are base substitutions and base additions or deletions. In base substitutions, one base pair nucleotide was replaced by another, and it is divides into two subtypes: transition and transversion. A transition means purine was replaced by purine: either A to G, or G to A; or pyrimidine was replaced by pyrimidine: either C to T, or T to C. And in the opposite, a transversion means pyrimidine was replaced by purine: C to A, C to G, T to A, or T to G; or purine was replaced by pyrimidine: A to C, A to T, G to C, or G to T [4].

Spontaneous errors in replication of enzyme are related to point mutations. Each nucleotide base naturally exits in two alternative tautomers. Tautomer means structural isomers in dynamic equilibrium. Thymine and guanine have two tautomers which have the keto and enol forms, and adenine has two isomers which are amino and imino forms. The common forms are keto-thymine, amino-adenine, and keto-guanine. The rare form enol-

thymine will bind with guanine not adenine. The rare form amino-adenine will combine with cytosine not thymine, and enol-guanine will link with thymine not cytosine (Fig.1.2). Individual molecules occasionally undergo a shift from one tautomer to the other. After the inserted error of the rare tautomer to replication fork, the rare tautomer will revert to its more common form, and point mutation will occur [3].

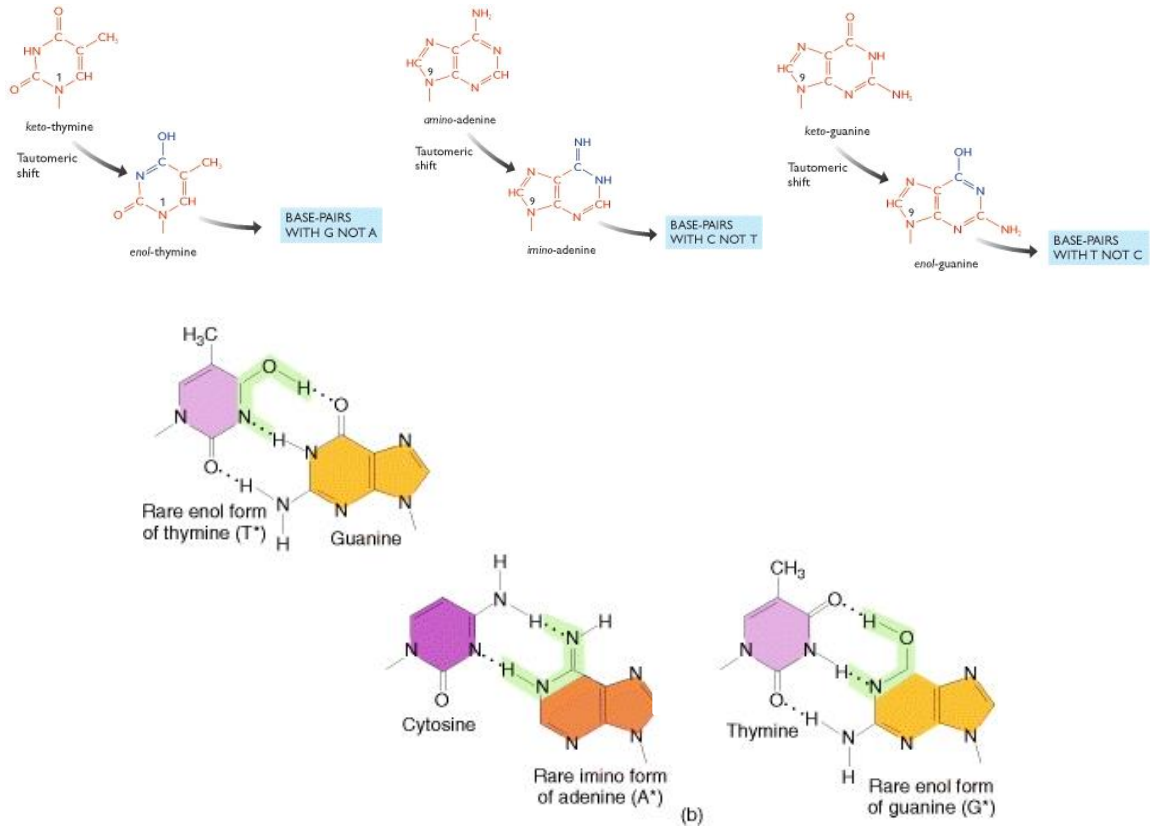

Figure 1.2: Alternative tautomers and the difference pairing characteristics of the two tautomeric forms [3, 4].

Mutations are also caused by chemical and physical mutagens [4]. Some mutagens act as analog bases, and are mistakenly inserted to replication fork (Fig.1.3). Some mutagens

directly insert to DNA. And some mutagens stimulate cells to synthesize one or more chemical, therefore they are indirectly related to the mutations [3].

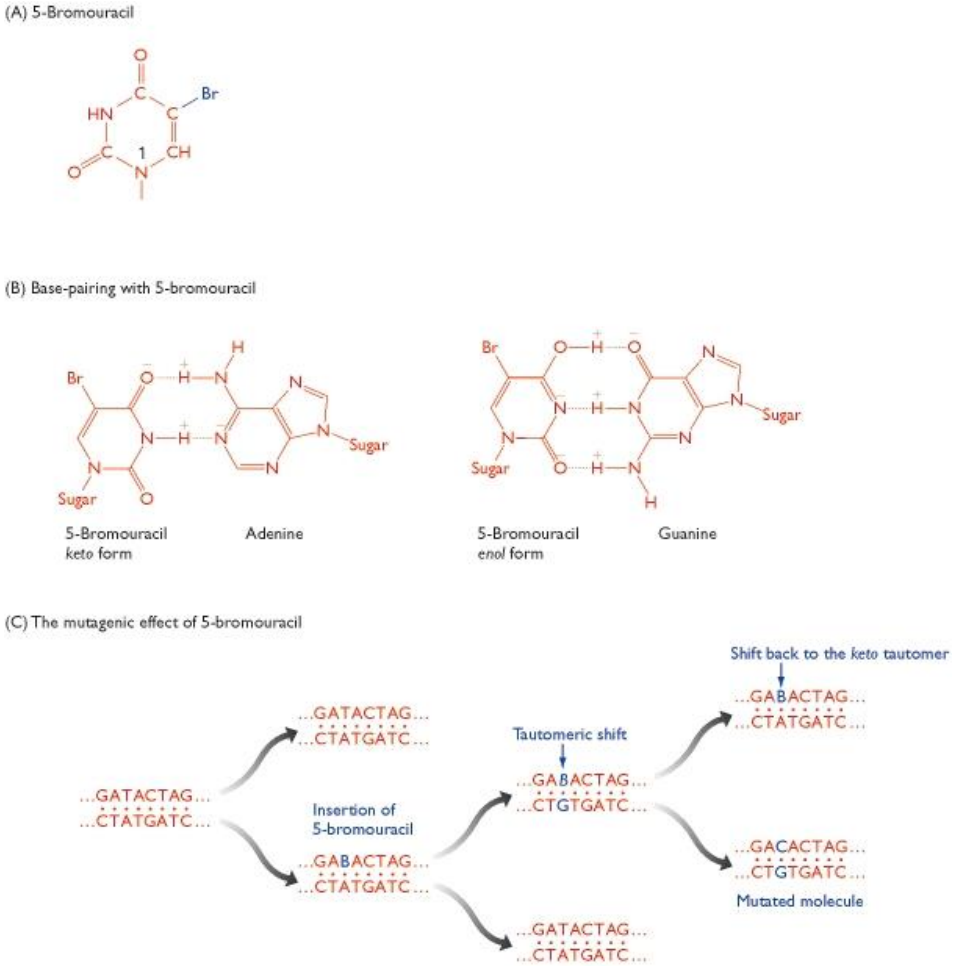

Figure 1.3: 5-bromouracil and its effect [3].

T>C or G>A point mutations were related with many human diseases [9] as listed in Table1.1 below. These T>C or G>A mutations were occurred in nuclear genes, and mitochondrial mutations were not listed in here. New detected diseases are being reported every year.

Table 1.1: T>C or G>A substitutions causing human genetic diseases [9].

N_0	Disease state	Gene symbol	Base change	Amino acid	Codon	Author	Journal	Vol.	Page	Year
1	ADA deficiency	ADA	CTG-CCG	Leu-Pro	107	Hirschhorn	*PNAS*	87	6171	1990
2	ADA deficiency	ADA	AAA-AGA	Lys-Arg	80	Valerio	*EMBO J*	5	113	1986
3	Adrenal hyperplasia	CA21HB	AAC-AGC	Asn-Ser	494	Rodrigues	*EMBO J*	6	1653	1987
4	APRT deficiency	APRT	ATG-ACG	Met-Thr	136	Hidaka	*JCI*	81	945	1988
5	Albinism, ocul. (1)	TYR	GAC-GGC	Asp-Gly	42	King	*MBM*	8	19	1991
6	Albumin Komagome 2	ALB	CAT-CGT	His-Arg	128	Madison	*PNAS*	88	9853	1991
7	Aldolase A defic.	ALDA	GAT-GGT	Asp-Gly	128	Kishi	*PNAS*	84	8623	1988
8	Amyloid polyneur.	PALB	TAC-TGC	Tyr-Cys	114	Ueno	*BBRC*	169	143	1990
9	Amyloid prealbumin	PALB	GTG-GCG	Val-Ala	30	Johns	*CLIN GENET*	41	70	82
10	Androgen insens. syn.	AR	TAC-TGC	Tyr-Cys	761	McPhaul	*JCI*	87	1413	1991
11	Antithrombin III def.	AT3	TTC-TCC	Phe-Ser	402	Olds	*TH*	65	670	1991
12	Antitrypsin α1 def.	PI	CTG-CCG	Leu-Pro	41	Tahahashi	*JBC*	263	15528	1988
13	Antitrypsin α1 def.	PI	GTG-GCG	Val-Ala	213	Nukiwa	*JBC*	261	15989	1986
14	Chr. Granulomat. dis.	CYBB91	CAT-CGT	His-Arg	101	Bolscher	*BLOOD*	77	2482	1991
15	Cystic fibrosis	CFTR	TAT-TGT	Tyr-Cys	913	Vidaud	*HUM*	85	446	1990

							GENET			
16	Elliptocytosis	SPTA	CTG-CCG	Leu-Pro	207	Gallagher	*JCI*	89	892	1992
17	Elliptocytosis	SPTA	AAG-AGG	Lys-Arg	48	Floyd	*BLOOD*	78	1364	1991
18	Epidermolysis bull	KRT14	CTG-CCG	Leu-Pro	384	Bonfias	*SCIENCE*	254	1202	1991
19	G6PD deficiency	G6PD	CAC-CGC	His-Arg	32	Chao	*NAR*	19	6056	1991
20	G6PD deficiency	G6PD	CTG-CCG	Leu-Pro	968	Beutler	*BLOOD*	74	2550	1989
21	Galactosaemia	GALT	CTG-CCG	Leu-Pro	195	Reichardt	*GENOMICS*	12	596	1992
22	Galactosaemia	GALT	CAG-CGG	Gln-Arg	188	Reichardt	*AJHG*	49	860	1991
23	Gangliosidosis GM1	GLB1	ATC-ACC	Ile-Thr	51	Yoshida	*AJHG*	49	435	1991
24	Gangliosidosis GM1	GLB1	TAT-TGT	Tyr-Cys	316	Yoshida	*AJHG*	49	435	1991
25	Gaucher's disease (1)	GBA	AAC-AGC	Asn-Ser	370	Tsuji	*PNAS*	85	2349	1988
26	Gaucher's disease (2)	GBA	CTG-CCG	Leu-Pro	444	Tsuji	*NEJM*	316	570	1987
27	Gyrate atrophy	OAT	CTT-CCT	Leu-Pro	402	Mitchell	*PNAS*	86	197	1989
28	HPRT deficiency	HPRT	CTA-CCA	Leu-Pro	40	Davidson	*JCI*	84	342	1989
29	HPRT deficiency	HPRT	ATT-ACT	Ile-Thr	41	Davidson	*AJHG*	48	951	1991
30	HPRT deficiency	HPRT	ATG-ACG	Met-Thr	56	Skopeck	*HUM GENET*	85	111	1990
31	HPRT deficiency	HPRT	TTG-TCG	Leu-Ser	130	Gibbs	*PNAS*	86	1919	1989
32	HPRT deficiency	HPRT	ATT-ACT	Ile-Thr	131	Davidson	*AJHG*	48	951	1991
33	HPRT deficiency	HPRT	GAT-GGT	Asp-Gly	52	Lightfoot	*HUM GENET*	88	695	1992
34	HPRT deficiency	HPRT	ATT-ACT	Ile-Thr	182	Tarle	*GENOMICS*	10	499	1991
35	HPRT deficiency	HPRT	GAT-GGT	Asp-Gly	200	Davidson	*JBC*	264	520	1989
36	HPRT deficiency	HPRT	CAT-CGT	His-Arg	203	Tarle	*GENOMICS*	10	499	1991
37	Haemoglobin	HBB	CAT-CGT	His-Arg	117	Kutlar	*HUM*	86	591	1991

	Malta						*GENET*			
38	Haemolytic anaemia	PGK	CTG-CCG	Leu-Pro	88	Maeda	*BLOOD*	77	1871	1991
39	Haemophilia A	F8	TTC-TCC	Phe-Ser	293	Higuchi	*PNAS*	88	7405	1991
40	Haemophilia A	F8	TTG-TCG	Leu-Ser	2166	Levinson	*AJHG*	46	53	1990
41	Haemophilia A	F8	GAA-GGA	Glu-Gly	272	Youssoufia	*AJHG*	42	867	1988
42	Haemophilia A	F8	AAA-AGA	Lys-Arg	425	Higuchi	*PNAS*	88	7405	1991
43	Haemophilia A	F8	TAT-TGT	Tyr-Cys	473	Higuchi	*PNAS*	88	7405	1991
44	Haemophilia A	F8	GAT-GGT	Asp-Gly	542	Higuchi	*PNAS*	88	7405	1991
45	Haemophilia A	F8	TAT-TGT	Tyr-Cys	1680	Traystman	*GENOMICS*	6	293	1990
46	Hepatic lipase def.	HL	AAT-AGT	Asn-Ser	193	Hegele	*BBRC*	179	78	1991
47	Insulin resistance	INSR	CTG-CCG	Leu-Pro	233	Klinkham.	*EMBO J*	8	2503	1989
48	Isovaleric acidaemia	IVD	CTA-CCA	Leu-Pro	13	Vockley	*AJHG*	49	147	1991
49	LDLR deficiency	LDLR	TAT-TGT	Tyr-Cys	807	Davis	*CELL*	45	15	86
50	Laron dwarfism	GHR	TTT-TCT	Phe-Ser	96	Amselem	*NEJM*	321	989	1989
51	Leprechaunism	INSR	CAC-CGC	His-Arg	209	Kadowaki	*JCI*	86	254	1990
52	Leukocyte adhes. Def.	LFA1	CTA-CCA	Leu-Pro	149	Wardlaw	*JEM*	172	335	1990
53	Lipoprt. lipase def.	LPL	ATT-ACT	Ile-Thr	194	Henderson	*JCI*	87	2005	1991
54	Lipoprt. lipase def.	LPL	GAT-GGT	Asp-Gly	158	Ma	*JBC*	267	1918	1992
55	LCAM deficiency	LCAM	AAT-AGT	Asn-Ser	351	Nelson	*JBC*	267	3351	1992
56	MCAD deficiency	MCAD	ATA-ACA	Ile-Thr	375	Yokota	*AJHG*	49	1280	1991
57	Marfan syndrome	COL1A2	CAG-CGG	Gln-Arg	618	Phillips	*JCI*	86	1723	1990
58	Methaemoglobin	DIA1	CTG-CCG	Leu-Pro	148	Katsube	*AJHG*	48	799	1991
59	Methylmalonicac	MCM	CAT-CGT	His-Arg	532	Crane	*JCI*	89	385	1992

	id.									
60	Neurofibromatosis (1)	NF1	CTG-CCG	Leu-Pro		Cawthon	*CELL*	62	193	1990
61	OTC deficiency	OTC	CTA-CCA	Leu-Pro	45	Grompe	*AJHG*	48	212	1991
62	OTC deficiency	OTC	CTT-CCT	Leu-Pro	111	Grompe	*AJHG*	48	212	1991
63	Phenylketonuria	PAH	TTG-TCG	Leu-Ser	48	Konecki	*HUM GENET*	87	389	1991
64	Phenylketonuria	PAH	TTG-TCG	Leu-Ser	255	Hofman	*AJHG*	48	791	1991
65	Phenylketonuria	PAH	CTG-CCG	Leu-Pro	311	Licht-K	*BIOCHEM*	27	2881	1988
66	Phenylketonuria	PAH	TAT-TGT	Tyr-Cys	204	Wang	*GENOMICS*	10	449	1991
67	Phenylketonuria	PAH	GAA-GGA	Glu-Gly	221	Konecki	*HUM GENET*	87	389	1991
68	Phenylketonuria	PAH	TAC-TGC	Tyr-Cys	414	Okano	*NEJM*	324	1232	1991
69	Pompe disease	GAA	ATG-ACG	Met-Thr	318	Zhong	*AJHG*	49	635	1991
70	Retinitis pigmentosa	RDS	CTG-CCG	Leu-Pro	185	Kajiwara	*MATURE*	354	480	1991
71	Retinitis pigmentosa	RHO	TAC-TGC	Tyr-Cys	178	Sung	*PNAS*	88	6481	1991
72	Retinitis pigmentosa	RHO	GAC-GGC	Asp-Gly	190	Sung	*PNAS*	88	6481	1991
73	Ster.18-hydrox. def.	CYP18	GTG-GCG	Val-Ala	386	Mitsuuchi	*BBRC*	182	974	1992
74	Thalassaemia α	HBA2	ATG-ACG	Met-Thr	-1	Piratsu	*JBC*	259	12315	1984
75	Thalassaemia α	HBA2	CTG-CCG	Leu-Pro	125	Goossens	*NATURE*	296	864	1982
76	Thalassaemia β	HBB	CTG-CCG	Leu-Pro	110	Kobayshi	*BLOOD*	70	1688	1987
77	Thalassaemia δ	HBD	CTG-CCG	Leu-Pro	141	Trifillis	*BLOOD*	78	3298	1991
78	Wilm` tumor	WT1	GAC-GGC	Asp-Gly	396	Pelletier	*CELL*	67	437	1991

1.2. Genetic therapy

Gene therapy is attempts to correct of defective genes by getting the new, or replacement genes into the patient's target cells [9, 10]. Germ line gene therapy and somatic gene therapy are two types of gene therapy. The first type is the changes in germ cells (including sperm and egg) by the introduction of functional genes. These changes were integrated into genome of germ cells, therefore these modifications would be heritable [11-13]. In the second type, the therapeutic genes are passed in the somatic cells of patient, therefore these changes were restricted to individual patient, and they could not be inherited [14-17]. Both germ line gene therapy and somatic gene therapy were used to replace defective gene, or block the effects of unwanted ones by introduction of a counteracting gene [18].

To delivery therapeutic vectors there are two techniques were used. The first one is *ex-vivo*. And the second one is *in-vivo* [19]. In *ex-vivo* technique, the patient's cells were extracted. Next, the therapeutic vectors were transfected to the patient's cells. And again these transfected cells were refused to the patient to product defected proteins. In *in-vivo* technique, the inserted vector was injected to the patient's blood stream to seek out, and link with targeted cells.

Some vectors were used to bring inserted genes. The viral vector and non-viral vector are two types of vector. In the former, one or more genes in genome of viral system were

removed, and replaced by the inserted gene [20]. Retrovirus [21], Adenovirus [22], Adeno-associated virus and Herpes simple virus [23] were already reported for gene transfer vehicles. In that case of non-vector, there are several methods such as direct naked DNA injection [24], electroporation (creation of electric field induced pores in plasma membrane), sonoporation (ultrasonic frequencies to disrupt cell membrane), magnetofection (use of magnetic particle complexed with DNA), gene guns (shoots DNA coated gold particles into cells by using high pressure), and receptor mediated gene transfer [25]. Genetic therapy is very promising, but it also has many disadvantages such as insertional mutagenesis, uncontrol cell division, etc. [26-29].

1.3. Natural RNA editing

RNA editing is the modification of nucleotide sequences of RNA [30]. As the according results, the encoding DNA was changed. Therefore, RNA editing is a post-transcriptional process to generate the diversity of RNA and protein [31]. RNA editing is carried out in the cell nucleus, cytosol, as well as mitochondrial, and plastids [32].

There are five type of RNA editing. It includes uridine-insertion/deletion, C- insertion and dinucleotide insertion, sno RNA-mediated nucleotide modification of rRNAs, tRNA editing, C-to-U substitution, and A-to-I editing [33]. In these categories, C-to-U substitution and A-to-I editing was shown to occur in mammals, and particularly in human. Both cases have the same of biochemical mechanisms, but the difference of molecular machineries [34].

C-to-U editing

Among RNA editing targets, the standard instance for C-to-U editing is apolipoproteinB (apoB) RNA [35]. Apo B has important function in lipoprotein metabolism to transport cholesterol and triglyceride in the blood. Apo B exits in two isoforms, which are apoB100 and apoB48 [36]. A single C to U substitution (C6666U) changes an arginine-specifying CAA codon into a premature UAA stop signal [37]. Generation of the UAA (stop) codon produced truncated apoB48 rather than full-length apoB100 (Fig.1.4). ApoB100 is synthesized in the liver, whereas apoB48 is edited in the small intestines. ApoB100 (512kDa) has two domains. One is lipoprotein assembly domain and the other is low density lipoproteins (LDL) receptor domain. It is required for the synthesis, assembly and secretion of very low density lipoproteins (VLDL); and the maturation products intermediate density lipoproteins (IDL), and low density lipoproteins (LDL) [38]. ApoB48 has 48% identification with full-length apoB 100. And it is the major protein component of triglyceride-rich chylomicrons [39, 40].

ApoB mRNA editing is needed the presence of the cis-acting sequence elements on apoB RNA and a multicomponent protein complex (editosome). The cis-acting sequence elements include a mooring sequence, and 5’ and 3’ efficiency elements (Fig.1.5) [37, 42]. The editosome are apobec1 (apoB mRNA editing enzyme catalytic subunit 1), and unknown auxiliary complementary factor (ACF). Apobect1 (27kDa) is one member of

family of cytidine deaminase enzyme [43-47]. The same with other cytidine deaminase enzymes, apobect1 is the zinc-dependent proteinacious deaminase activity [48, 49].

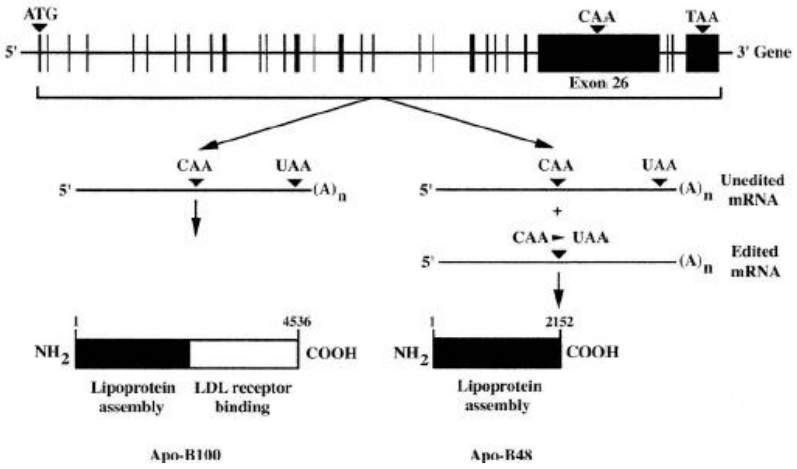

Figure 1.4: The apoB gene (14kb), and the two forms of apoB100 and apoB48 [41].

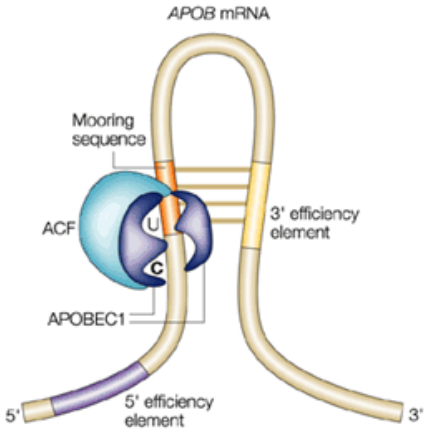

Figure 1.5: Apobec1 binds to apoB mRNA together with unknown auxiliary complementary factor (ACF), and catalyses the C>U deamination. The cis-acting sequence elements are a mooring sequence, and 5' and 3' efficiency elements [42].

A-to-I editing

RNA editing of the α-amino-3-hydroxy-5-methyl-4-isoxazole-propionic (AMPA) receptor is one clear example of A-to-I editing. AMPA receptor is one of three distinct types of ion-transporting glutamate receptor (GluRs) (including AMPA, N-methyl D-aspartate-NMDA and kainite-KA receptors) [50-52]. It is popular in central nervous system (CNS) [53].

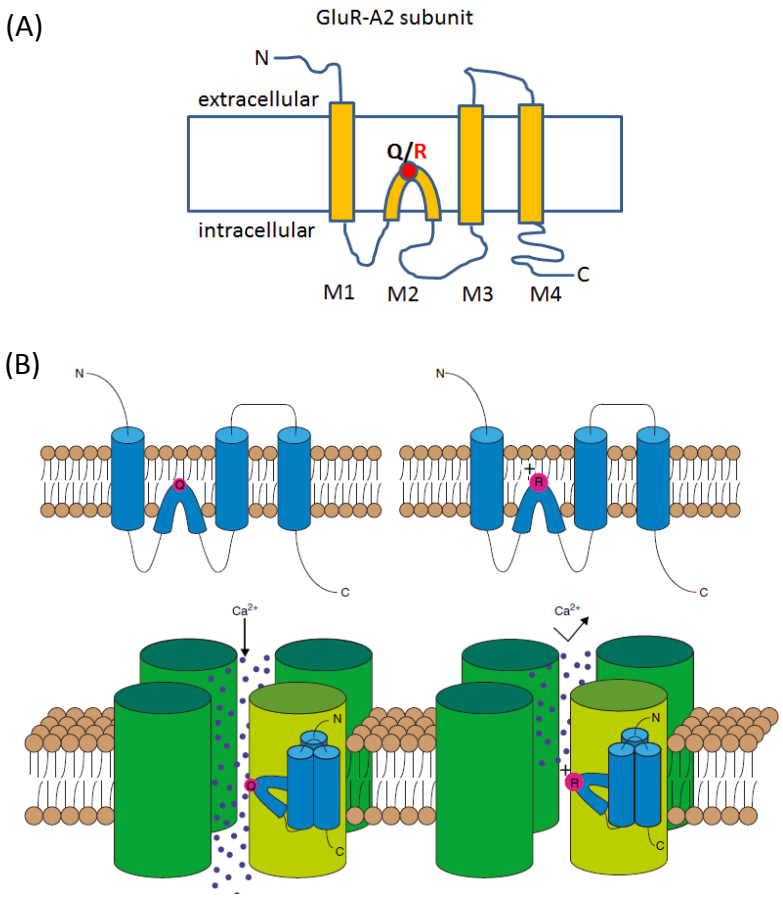

Figure 1.6: Secondary structure of the GluR-A2 subunit with three transmembrane domains. The Q/R editing site is located in second membrane domain (A) and controls Ca^{2+}-permeability of the AMPA receptor site (B) [34].

Firstly, it will be activated by the excitatory neurotransmitter L-glutamate. Next, AMPA receptor will allow the influx of Na^+ and Ca^{2+} ions into the postsynaptic density [53]. AMPA receptor has four subunits which are GluR-A1, GluR-A2, GluR-A3 and GluR-A4 [54]. The mRNA that encoded for GluR-A2 undergoes RNA editing at glutamine/arginine (Q\R) site [55, 56]. In addition, the type of GluR-A2 will decide the Ca^{2+}-permeability (Fig.1.6B). RNA editing changes a glutamine codon (Gln; Q) to arginine (Arg; R) in membrane region 2 (M2) of GluR-A2 receptor (Fig.1.6A) [53, 57].

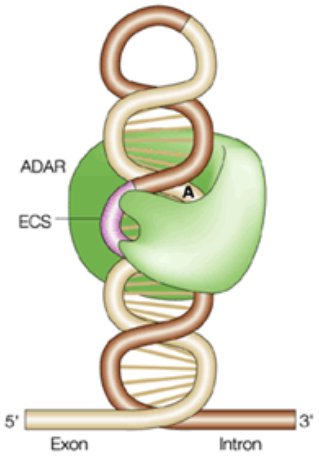

Figure 1.7: Adenosine deaminases that act on RNAs (ADARs) recognize duplex RNA. The recognized duplex RNA is formed between the editing site and editing site complementary sequence (ECS) in a downstream intron. The enzymes bind to the double strand (ds) RNA through their dsRBDs and deaminase, and catalyze specific adenosine to inosine deamination [42].

AMPA RNA editing requires the presence of base-pair structure and the adenosine deaminase acting on RNA 2 (ADAR2) enzyme. Base-pair structure was formed between the exon sequences near the editing site and the downstream intron (Fig.1.7) [58-61]. ADAR2 enzyme is one member of double strand (ds) RNA adenosine deaminase enzyme.

The same with other dsRNA adenosine deaminase enzymes, ADAR2 also is the zinc-dependent proteinacious deaminase activity [48, 49]

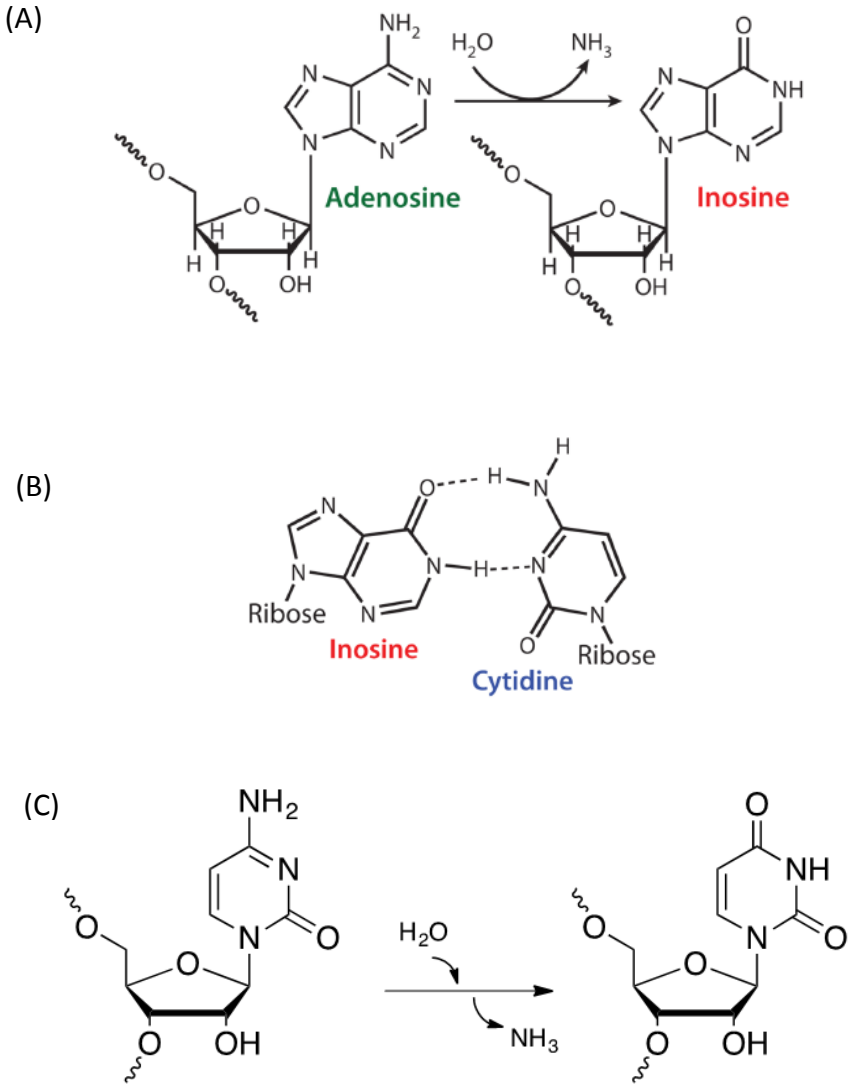

Figure 1.8: A hydrolytic deamination reaction converts adenosine to inosine (A) and cytosine to uridine (C). Inosine base pairs with guanosine (B) [64].

During the RNA editing, the base conversions were carried out by hydrolytic deamination, and were catalyzed by deaminase enzymes (Fig.1.8) [62, 63].

The regulation of RNA editing is very diversity and complex. For apobect1 enzyme, there are several regulatory mechanisms such as the use of alternative promoters, alternative splicing, and variety of dietary and pharmacological manipulations [65, 37]. For the regulation of ADAR2 enzyme, an auto-regulation feed-back mechanism and alternative splicing was observed [66, 49].

Abnormal RNA editing can cause human diseases, and pathophysiology [67, 68]. The miss-regulation of RNA editing was showed having some connection to cancer. It caused the tumor genesis by either inactivating a tumor suppressor or activating oncological gene [69-71, 67] for example a specific deficiency in A-to-I editing of GluR receptor is related to human brain cancer [72, 73]. Neurological disorders and behavior were also caused by defects or deregulation in RNA editing [74-76].

1.4. Site-directed, chemical, non-enzymatic RNA editing

Recently, non-enzymatic, site-directed editing was interesting because it has potential application for treatment of point mutation diseases. This method is simple and un-expensive comparing with enzymatic RNA editing. Prof. Fujimoto and colleagues were firstly reported this method, and by using a short 20-mer as target, they showed that the C-to-U substitution was effective and sequence-specific *in vitro* [77]. They designed and

studied ^{CV}U and ^{CNV}K modified oligonucleotides for DNA and RNA editing [77, 78]. These modified ODNs were synthesized according to the standard phosphoramidite chemistry on a DNA synthesizer using phosphoroamidite with the post-modification procedure after ODN synthesis [77].

In DNA editing, they showed that these modified oligonucleotides covalently binds with the target DNA strand via a [2+2] photocycloaddition between photoreactive nucleoside and deoxycytidine at a specific position in the target DNA on 366nm UV irradiation. Next, heating for deamination and 312nm UV irradiation for photosplitting was carried out to artificially edited target DNA with cytosine to uracil photo-transition (Fig.1.9) [77].

In RNA editing, the mechanism was not yet showed but the photo-transition process also included four main step reactions. The step 1, the hybridization between the modified oligonucleotide and the target RNA was generated. The step 2, photo-crosslinking between them was carried out by 366nm UV irradiation. The step 3, heat treatment was done to deamination. The final step, the target RNA and the modified oligonucleotide was separated by photosplitting (Fig.1.10) [77, 78].

Non-enzymatic, site-directed editing showed that it has high efficiency without any side reaction [77, 78].

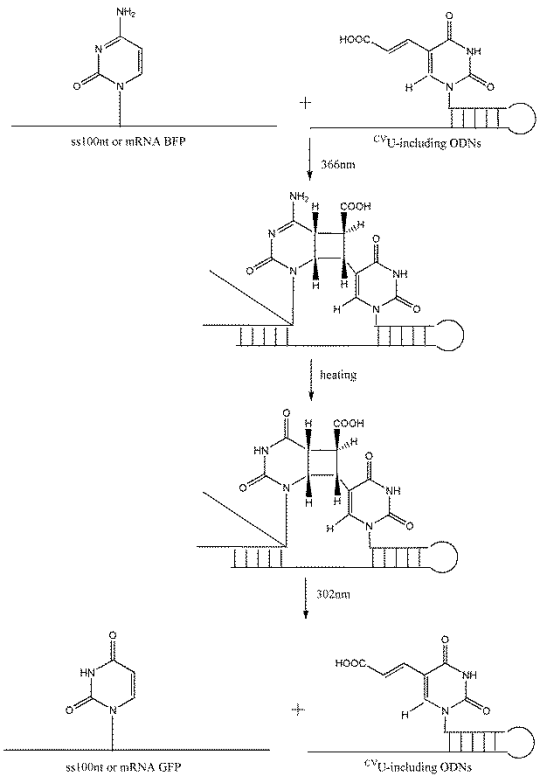

Figure 1.9: Site-directed, chemical RNA editing by using ^{CV}U-containing ODNs [77].

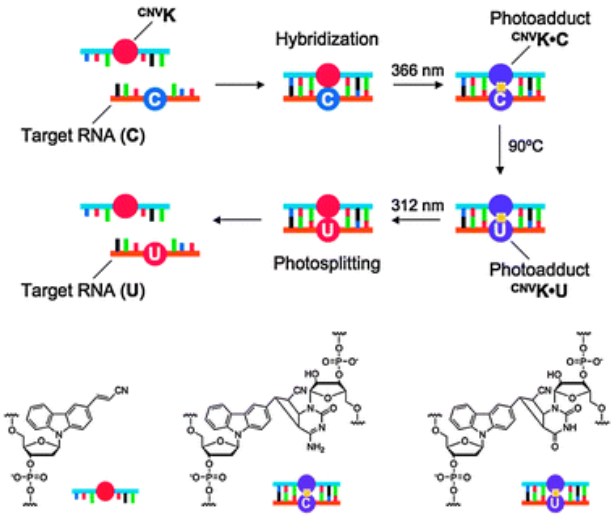

Figure 1.10: Site-directed, chemical RNA editing by using ^{CNV}K-containing ODNs [78].

The main objectives of my study are:-

1. To investigate the application of site-directed, chemical RNA editing for treatment of Leigh syndrome.
2. To investigate the change of blue fluorescent protein to green fluorescent protein as model by chemical RNA editing as novel strategy in genetic restoration.
3. To survey the relationships between the primary structures and deamination efficiency of carboxyvinyldeoxyudenine ODNs (^{CV}U-containing ODNs) on chemical RNA editing for genetic restoration. From these results, the suitable, effective and optimum ODN will be designed for any T>C or G>A caused diseases.

1.7 REFERENCES

[1] Pearson H: **Genetics: what is a gene?** *Nature* **2006**, 441 (7092): 398-401.

[2] Griffiths AJF, Wessler SR, Lewontin RC, Gelbart WM, Suzuki DT, Miller JH: **Introduction to genetic analysis**. 8th edition, page 227-254.

[3] Brown TA: **Genomes**

[4] Griffiths AJF, Gelbart WM, Miller JH, Lewontin RC: **Modern genetic analysis**

[5] Kimura M, Ohta T: **Mutation and evolution at the molecular level**. *Genetics* **1973**, 73 (suppl.): 19-35.

[6] Stamatoyannopoulos G, Nute PE: **De novo mutations producing unstable Hbs or Hbs**. *M. Hum. Genet.* **1982**, 60: 181-188.

[7] Neel JV, Satoh C, Goriki K, Fujita M, Takahashi N, Asakawa J-I, Hazama R: **The rate with which spontaneous mutation alters the electrophoretic mobility of polypeptides**. *Proc. Natl. Acad. Sci. USA* **1986**, 83: 389-393.

[8] Cooper DN, Krawczak M: **Human gene mutation**. *Bios Science Publishers* **1994**, p331-387

[9] Miller AD: **Human gene therapy comes of age.** *Nature* **1992**, 357: 455-460.

[10] Verma IM, Weitzman MV: **GENE THERAPY: Twenty-First Century Medicine**. *Annurev.biochem.* 74: 711-738.

[11] Johnson J, Canning J, Kaneko T, Pru JK, Tilly JL: **Germline stem cells and follicular renewal in the postnatal mammalian ovary**. *Nature* **2004**, 428: 145-150.

[12] Prelle K, Zink N, Wolf E: **Pluripotent stem cells-model of embryonic development, tool for gene targeting and basis of cell therapy**. *Anat. Histol. Embryol.* **2002**, 31: 169-186.

[13] Misra S: **Human gene therapy: a brief overview of the genetic revolution**. *JAPI* **2013**, 61: 127-133.

[14] Friedmann T: **Progress toward human gene therapy**. *Science* **1989**, 24(4): 1275-1281.

[15] Crystal RG: **Transfer of genes to humans: early lessons and obstacles to success**. *Science* **1995**, 270: 404-410.

[16] Cross D, Burmester JK: **Gene therapy for cancer treatment: past, present and future**. *Clinical Medicine & Research* 4(3): 218-227.

[17] Bank A: **Human somatic cell gene therapy**. *BioEssays* **1996**, 18(12): 999-1007.

[18] Verma IM, Somia N: **Gene therapy-promises, problems and prospects**. *Nature* **1997**, 389: 239-242.

[19] Romano G, Pacilio C, Giurdano A: **Gene transfer technology in therapy: current application and future goals.** *Stem Cells* **1999**, 17: 191-202.

[20] Walther W, Stein U: **Viral vector for gene transfer: a review of their use in the treatment of human disease**. *Drug* **2000**, 60:249-271.

[21] Rochat T, Morris MA: **Viral vector for gene therapy**. *J Aerosol Med* **2002**, 15: 229-235.

[22] Vorburger SA, Hunt KK: **Adenoviral gene therapy**. *The Oncologist* **2002**, 7: 46-59.

[23] Varghese S, Robkin DS: **Oncolytic herpes simplex virus vector for cancer virotherapy**. *Cancer Gene Therapy* **2002**, 9: 967-78.

[24] Wolff JA, Malone RW, Williams P, et al: **Direct gene transfer into mouse muscle i*n vivo***. *Science* **1990**, 247: 1465-68.

[25] Wagner E, Curiel D, Cotton M: **Delivery of drugs, proteins and genes using transferring as a ligand for receptor-mediated endocytosis**. *Adv. Drug. Deliv. Rev.* **1994**, 14: 113-135.

[26] Verma IM, Somia N: **Gene therapy-promisees, problems and prospects**. *Nature* **1997**, 389: 239-242.

[27] Dullmann BC, LI J, Fehse Z, Meyer B, Williams JDA, Kalle CV: **Side effects of retroviral gene transfer into hematopoietic stem cells**. *Blood* **2003**, 101(6): 2099-2114.

[28] Zychlinski D, Schambach A, Modlich U, Maetzig T, Meyer J, Grassman E, Mishra A, Baum C: **Physiological promoters reduce the genotoxic risk of integrating gene vectors.** *Molecular Therapy* **2008**, 16(4): 718-715.

[29] Kaufmann KB, Buning H, Galy A, Schambach A, and Crez M: **Gene therapy on the move**. *EMBO Mol. Med.* **2013**, 5: 1642-1661.

[30] Gray MW: **Evolution origin of RNA editing**. *Biochemistry* **2012**, 51(26): 5235-5242.

[31] Decher N, Netter MF, Streit AK: **Putative impact of RNA editing on drug discovery**. *Chemical Biology & Drug Design* **2013**, 81(1): 13-21.

[32] Simpson L, Emeson RB: **RNA editing**. *Annual Review of Neuroscience* **1996**, 19: 27-52.

[33] Tang W, Fei Y, Page M: **Biological significance of RNA editing in cells**. *Molecular Biotechnology* **2012**, 52(1): 91-100.

[34] Maas S, Rich A: **Changing genetic information through RNA editing**. *BioEssays* **2000**, 22: 790-802.

[35] Blanc V, Davidson NO: **APOPEC-1-mediated RNA editing**. *Wiley Interdiscip. Rev.: Syst. Biol. Med.* **2010**, 2: 594-602.

[36] Kane JP, Apolipoprotein B: **structural and metabolic heterogeneity**. *Anu. Rev. Physiol* **1983**, 45: 637-650.

[37] Niswender CM: **Recent advances in mammalian RNA editing**. *Cell Mol Life Sci*. **1998**, 54: 946-964.

[38] Ginsberg HN, Fisher EA: **The ever-expanding role of degradation in the regulation of apolipoprotein B metabolism**. *J Lipid Res.* **2009**, 50(suppl): s162-s166.

[39] Innerarity TL, Boren J, Yamanaka S, Olofsson S-O: **Biosynthesis of apolipoprotein B48-containing lipoproteins.** *J Biol. Chem.* **1996**, 271: 2353-2356.

[40] Chan L, Chang BH, Nakamuta M, Li WH, Smith LC: **Apobec-1 and apolipoprotein mRNA editing.** *Biochim. Biophys. Acta* **1997**, 1345: 11-16.

[41] Chester A, Scott J, Anant S, Navaratnam N: **RNA editing: cytidine to uridine conversion in apolipoprotein B mRNA.** *Biochimca et Biophysica Acta* **2000**, 1494: 1-13.

[42] Keegan LP, Gallo A, O'Connell MA: **The many roles of an RNA editor.** *Nature Reviews Genetics* **2001**, 2: 869-878.

[43] Teng B, Burant CF, Davidson NO: **Molecular cloning of an apolipoprotein B messenger RNA editing protein.** *Science* **1993**, 260: 1816-1819.

[44] Hadjiagapiou C, Giannoni F, Funahashi T, Skarosi SF, Davidson NO: **Molecular cloning of a human small intestinal apolipoprotein B mRNA editing protein.** *Nucleic Acids Res.* **1994**, 22: 1874-1879.

[45] Johnson DF, Poksay KS, Innerarity TI: **The mechanism for Apo-B mRNA editing is deamination.** *Biochem. Biophys. Res. Commun* **1993**, 195:1204-10

[46] Dnscoll DM, Zhang Q: **Expression and characterization of p27, the catalytic subunit of the apolipoprotein B mRNA editing enzyme.** *J. Biol. Chem.* **1994**, 269: 19843-19847.

[47] Yamanaka S, Poksay KS, Balestra ME, Zeng G-Q, Innerarity TL: **Cloning and mutagenesis of the rabbit apoB mRNA editing protein. A zinc motif is essential for catalytic activity, and noncatalytic auxiliary factor(s) of the editing complex are widely distributed.** *J. Biol. Chem.* **1994**, 269: 21725-21734.

[48] Maas S, Melcher T, Seeburg PH: **Mammalian RNA-dependent deaminases and edited mRNAs.** *Curr Opin Cell Biol* **1997**, 9:343-349.

[49] Rueter SM, Emeson RB: **Adenosine-to-inosine conversion in mRNA.** In: Grosjean H and Benne R, editors. **Modification and Editing of RNA.** *Washington, DC: American Society Microbiology Press*, **1998**, 343-361.

[50] Dubinsky JM, Rothman SM: **Intracellular calcium concentrations during "chemical hypoxia" and excitotoxic neuronal injury**. *J. Neurosci.* **1991**, 11: 2545-2551.

[51] Pizzi M, Ribola M, Valerio A, Memo M, Spano P: **Various Ca^{2+} entry blockers prevent glutamate-induced neurotoxicity.** *Eur. J. Pharmacol* **1991**, 209: 169-173.

[52] Randall RD, Thayer SA: **Glutamate-induced calcium transient triggers delayed calcium overload and neurotoxicity in rat hippocampal neurons.** *J. Neurosci.* **1992**, 12: 1882- 1895.

[53] Wrigh A, Vissel B: **The essential role of AMPA receptor GluR2 subunit RNA editing in the normal and diseased brain.** *Front Mol Neurosci* **2012**, 5: 34.

[54] Hollmann M, Hartley M, Heinemann S: **Ca^{2+} permeability of KA-AMPA-gated glutamate receptor channels depends on subunit composition.** *Science* **1991**, 252: 851-853.

[55] Kohler M, Burnashev N, Sakmann B, Seeburg PH: **Determinants of Ca^{2+} permeability in both TM1 and TM2 of high affinity kainate receptor channels: diversity by RNA editing.** *Neuron* **1993**, 10: 491-500.

[56] Brusa R, Zimmermann F, Koh DS, Feldmeyer D, Gass P, Seeburg PH, Sprengel R: **Early-onset epilepsy and postnatal lethality associated with an editing-deficient GluR-B allele in mice.** *Science* **1995**, 270: 1677-1680.

[57] Sommer B, Kohler M, Sprengel R, Seeburg PH: **RNA editing in brain controls a determinant of ion flow in glutamate-gated channels.** *Cell* **1991**, 67:11-19.

[58] Lomeli H, Mosbacher J, Melcher T, Hoger T, Geiger JRP, Kuner T, Monyer H, Huguchi M, Bach A, Seeburg PH: **Control of kinetic properties of AMPA receptor channels by nuclear RNA editing.** *Science* **1994**, 266 (5191): 1709-1713.

[59] Egebjerg J, Kukekov V, Heinemann SF: **Intron sequence directs RNA editing of the glutamate receptor subunit GluR2 coding sequence.** *Proc. Natl. Acad. Sci. USA* **1994**, 91: 10270-10274.

[60] Higuchi M, Single FN, Köhler M, Sommer B, Sprengel R, Seeburg PH: **RNA editing of AMPA receptor subunit GluR-B: a base-paired intron-exon structure determines position and efficiency.** *Cell* **1993**, 75(7):1361–1370.

[61] Herb A, Higuchi M, Sprengel R, Seeburg PH: **Q/R site editing in kainate receptor GluR5 and GluR6 pre-mRNAs requires distant intronic sequences.** *Proc. Natl. Acad Sci USA* **1996**, 93: 1875-1880.

[62] Bass BL, Weintraub H: **An unwinding activity that covalently modifies its double-stranded RNA substrate.** *Cell* **1988**, 55:1089–1098.

[63] Wagner RW, Smith JE, Cooperman BS, Nishikura K: **A double-stranded RNA unwinding activity introduces structural alterations by means of adenosine to inosine conversions in mammalian cells and Xenopus eggs.** *Proc. Natl. Acad. Sci. USA* **1989**, 86:2647–2651.

[64] Nishikura K: **Functions and regulation of RNA editing by ADAR deaminases.** *Annu rev Biochem.* **2010**, 79: 321-349.

[65] Nakamuta M, Oka K, Krushkal J, Kobayashi K, Yamamoto M, Li WH, Chan L: **Alternative mRNA splicing and differential promoter utilization determine tissue-specific expression of the apolipoprotein B mRNA editing protein (Apobec1) gene in mice. Structure and evolution of Apobec1 and related nucleoside/nucleotide deaminases.** *J Biol Chem* **1995**, 270: 13042-13056.

[66] Rueter SM, Dawson TR, Emeson RB: **Regulation of alternative splicing by RNA editing.** *Nature* **1999**, 399: 75-80.

[67] Maas S, Kawahara Y, Tamburro KM, Nishikura K: **A-to-I RNA editing and human disease.** *RNA Biol* **2006**, 3: 1–9.

[68] Schmauss C: **Regulation of serotonin 2C receptor pre-mRNA editing by serotonin.** *Int. Rev. Neurobiol* **2005**, 63: 83–100.

[69] Gallo A, Galardi S: **A-to-I RNA editing and cancer: from pathology to basic science.** *RNA Biol.* **2008**, 5.

[70] Paz N, Levanon EY, Amariglio N, Heimberger AB, Ram Z, Constantini S, Barbash ZS, Adamsky K, Safran M, Hirschberg A, Krupsky M, Ben-Dov I, Cazacu S, Mikkelsen T, Brodie C, Eisenberg E, Rechavi G: **Altered adenosine-to-inosine RNA editing in human cancer.** *Genome Res.* **2007**, 17, 1586–1595.

[71] Ishiuchi S, Tsuzuki K, Yoshida Y, Yamada N, Hagimura N, Okado H, Miwa A, Kurihara H, Nakazato Y, Tamura M, Sasaki T, Ozawa S: **Blockage of Ca^{2+}-permeable AMPA receptors suppresses migration and induces apoptosis in human glioblastoma cells.** *Nat. Med.* **2002**, 8, 971–978.

[72] Cenci C, Barzotti R, Galeano F, Corbelli S, Rota R, Massimi L, Di Rocco C, O'Connell MA, Gallo A: Down-regulation of RNA editing in pediatric astrocytomas: ADAR2

editing activity inhibits cell migration and proliferation. J. Biol. Chem. 2008, 283: 7251–7260.

[73] Maas S, Patt S, Schrey M, Rich A: **Underediting of glutamate receptor GluR-B mRNA in malignant gliomas.** *Proc. Natl. Acad. Sci. U. S. A.* **2001**, 98: 14687–14692.

[74] Kawahara Y, Grimberg A, Teegarden S, Mombereau C, Liu S, Bale TL, Blendy JA, Nishikura K: **Dysregulated editing of serotonin 2C receptor mRNAs results in energy dissipation and loss of fat mass.** *J. Neurosci.* **2008**, 28: 12834–12844.

[75] Singh M, Zimmernan MB, Beltz TG, Johnson AK: **Affect-related behaviors in mice misexpressing the RNA editing enzyme ADAR2.** *Physiol. Behav.* **2009**, 97: 446–454.

[76] Gardiner K, Du Y: **A-to-I editing of the 5HT2C receptor and behaviour.** *Brief Funct. Genomic Proteomic* **2006**, 5: 37–42.

[77] Fujimoto K, Matsuda S, Yoshimura Y, Matsumura T, Hayashi M, Saito I: **Site-specific transition of cytosine to uracil via reversible DNA photoligation**. *Chem. Commun.* **2006**, 30: 3223-3225.

[78] Fujimoto K, Konishi-Hiratsuka K, Sakamoto T, Yoshimura Y: **Site-specific photochemical RNA editing.** *Chem. Commun.* **2010**, 46: 7545-7547.

CHAPTER 2: THE APPLICATION OF SITE-DIRECTED CHEMICAL RNA EDITING FOR TREATMENT OF LEIGH SYNDROME

2.1. INTRODUCTION

Leigh syndrome (also known as subacute necrotizing encephalopathy, SNE) is a devastating, neurodegenerative disorder. It was characterized by almost identical brain changes, but it has clinical and genetic heterogeneity [1-3].

Leigh syndrome was firstly reported by Denis Leigh in 1951 [1]. In the general, Leigh syndrome patients display the decrease of central nervous system function because of focal, necrotizing lesions of the basal ganglia, diencephalon, cerebellum, or brainstem. Clinical phenomena include regression to psychomotor delay, weakness, hypotonia, truncal ataxia, intention tremor, and lactacidosis of the blood, cerebrospinal fluid, or urine [4].

Leigh syndrome was estimated about 1 of 40,000 live births [5]. This syndrome is regularly occurred infancy and early childhood [6], and rarely happened in adults [7]. Typically, it was expressed in the first 2 years of life [6].

The defection of the respiratory chain (particularly of complexes I, II, IV, or V), of coenzyme Q, or of the pyruvate dehydrogenase complex are related to Leigh syndrome [8]. Leigh syndrome is the mitochondrial disorders rather than nuclear disorders [9-11]. It

is maternally inherited disease. Most of the mutations lay within genes encoding Complex I and V (ATP6, ATP8) mitochondrial subunits [14].

One of the most frequently mutated mitochondrial genes in Leigh syndrome is ATPase6. The gene ATPase6 encodes for a subunit of respiratory-chain complex V. And the transversion T8993G was the most frequently mutation in this gene [12, 13].

No effective treatment was reported for Leigh syndrome until now [15]. Therefore, it is necessary to establish one approach for treatment of Leigh syndrome. Our new approach was based on chemical modification and transition of nucleotide [16]. We chose and used mitochondrial T8993C mutation of Leigh syndrome patient as model. To convert C8993U we carried out artificial, site-directed, chemical RNA editing. And after the C8993U transition, the Leigh syndrome sequences (mutated sequences) partly or totally were changed to wild-type sequences *in vitro*.

2.2. MATERIALS AND METHODS

2.2.1. Oligonucleotides and targets

The primary cultured fibroblast cells were obtained from the sample of muscle biopsy from one patient with Leigh syndrome, and this sample was kindly provided by Dr. Y. Goto, National Institute of Neuroscience, National Center of Neurology and Psychiatry under the approval by the local research ethics committee. These cells were grown in

Dulbecco's modified Eagle's medium/Ham's F-12 medium which was supplemented with 20% fetal bovine serum.

Whole genomic DNA (including mitochondrial DNA-mtDNA) and total RNA were purified from Leigh syndrome patient's cells by using Flexi Gene DNA Kit (Qiagen) or TRIzol Reagent (Invitrogen), respectively. Before the purification, these cells were washed three times by using ice-cold 1x PBS. Extraction steps were carried out according to supplier's protocols.

To prepare a full-length ATPase6 DNA, the high-fidelity PCR was done by using the previous purified whole DNA as template. The primer sequences were hmtDNA-ATP6-F: TTATGTGTTGTCGTGCAGGT and hmtDNA-ATP6-R: ATGAACGAAAATCTGTTCGC (Operon Biotechnologies). The PCR mixtures contained 50 ng of whole genomic DNA, 2 mM $MgCl_2$, 0.1 mM dNTPs, 1x Ex Taq Buffer, 0.25 U of Ex Taq (Takara Bio) and 2 pmol of each primer in 25 μL of total reaction mixtures. The PCR conditions were initially denatured at 94 °C for 5 min, followed by a cycle of denaturing at 94 °C for 30 sec, annealing at 51 °C for 30 sec and extension at 72 °C for 1 min. 40 cycles of amplification were performed. The PCR reactions were completed by 5 min extension at 72 °C. Then the full-length ATPase6 cDNA was subcloned into a pGEM-T Easy vector (Promega). Plasmid purification was carried out by using QIAGEN Plasmid Mini Kit (Qiagen) according to supplier's protocols. The full-length ATPase cDNA sequence was checked and confirmed by dideoxy sequencing (Applied Biosystems 3130xl Genetic Analyzer).

To prepare a double-stranded 681nt ATPase6, the high-fidelity PCR was done by using the previous purified plasmid as template. The primers were the same with previous PCR reaction (hmtDNA-ATP6-F and hmtDNA-ATP6-R). The PCR mixtures contained 50 ng of purified plasmid, 2 mM $MgCl_2$, 0.1 mM dNTPs, 1x Ex Taq Buffer, 0.25U of Ex Taq (Takara Bio) and 2 pmol of each primer in 25 μL of total reaction mixtures. The PCR conditions were initially denatured at 94 °C for 5 min, followed by a cycle of denaturing at 94 °C for 30 sec, annealing at 51 °C for 30 sec and extension at 72 °C for 1 min. 40 cycles of amplification were performed. The PCR reactions were completed by a 5 min extension at 72 °C. PCR reaction was following by phenol/chloroform extraction and ethanol purification. After purification, the concentration was measured by using ND-1000 Spectrophotometer (NanoDrop Technologies) and adjusted to 100 nM final concentration in 1x TE buffer.

Next, the previous purified plasmid was linearized with *ApaI* (Takara Bio). The recognized sequences of the restriction enzyme *ApaI* were presented in multi-cloning Site of the pGEM-T vector, but they were not presented in full-length ATPase6 cDNA. The digestion mixture contained 1 μg of purified plasmid, 10 U *ApaI*, 1x buffer L in 25 μL of total reaction mixture. Reaction mixture was incubated at 37 °C in overnight.

To prepare a single-stranded 731-nt ATPase6 (ss731-nt ATPase6), asymmetric PCR was carried out. The forward primer was hmtDNA-ATP6-F (5'-TTATGTGTTGTCGTGCAGGT-3'). The previous linearized plasmid was used as template. The asymmetric PCR mixture

contained 100 ng of the linearized plasmid, 2 mM $MgCl_2$, 0.6 mM dNTPs, 1x Ex Taq Buffer, 0.25 U of Ex Taq (Takara Bio) and 3 μM of hmtDNA-ATP6-F primer in 50 μL of total reaction mixture. The PCR conditions were initially denatured at 94 °C for 5 min, followed by a cycle of denaturing at 94 °C for 30 sec, annealing at 51 °C for 1 min and extension at 72 °C for 1 min. 90 cycles of amplification were performed. The PCR reactions were completed by 3 min extension at 72 °C. After asymmetric PCR reaction phenol/chloroform extraction and ethanol purification were done. Then, formamide was added to 80% final concentration and the mixture was heated at 70 °C for 3 min. Next, it was immediately quenched on ice water. The denatured mixture was applied to denaturing PAGE containing 7M Urea. A single-stranded 731-nt ATPase6 band was cut and purified by using crush and soak method. Finally, the concentration of purified ss731-nt ATPase6 was measured by using ND-1000 Spectrophotometer (NanoDrop Technologies) and adjusted to 100 nM final concentration in 1x TE buffer.

To prepare RNA 813-nt ATPase 6, *in vitro* transcription was carried out by using SP6 RNA polymerase (New England Biolabs) according to supplier's protocols. The previous linearized plasmid DNA was used as template. *In vitro* transcription was following by phenol/chloroform extraction and ethanol purification. After purification, formamide was added to 80% final concentration and the mixture was heated at 70 °C for 3 min. Next, it was immediately quenched on ice water. The denatured mixture was applied to denaturing PAGE containing 7M Urea. 813-nt ATPase6 RNA band was cut and purified by

using crush and soak method. The concentration was measured by using ND-1000 Spectrophotometer (NanoDrop Technologies) and adjusted to 100 nM final concentration.

Name	Sequences (5′→3′)
ODN1	^{CV}UGCGTGTTTTCACGCAGGGGCTATTGGTTG
ODN2	^{CV}UGCGTGTTTTCACGCAGGGGCTATTGGTTGAATGAGTA
ODN3	^{CV}UGCGTGACACTTTTGTGTCACGCAGGGGCTATTGGTTG
ODN4	^{CV}UGCGTGACACTTTTGTGTCACGCAGGGGCTATTGGTTGAATGAGTA
ODN5	^{CV}UGCGTGACTTTTGTCACGCAGGGGCTATTGGTTGAATGAGTA

Table 2.1: Sequences of 5 effecter ODNs. Each effecter ODN contains complementary part of boundary of the targeted C, hairpin loop structure and a photoresponsive ^{CV}U in 5′-terminus.

All oligodeoxynucleotides (ODNs) containing 5′-carboxyvinyl-2′-deoxyuridine (^{CV}U) (Table 2.1) were synthesized by an automated DNA synthesizer according to the conventional amidite chemistry [16]. An oligonucleotide from mitochondrial DNA from 8957 to 9028 (72 nucleotides) containing T8993C mutation, was used for synthetic target in trial experiments. 5′-^{CV}U-containing oligonucleotides were kindly provided by Professor, Dr. Kenzo Fujimoto, School of Materials Science, JAIST-Japan Advanced Institute of Science and Technology.

2.2.2. Photochemical deamination

The site-directed, chemical substitution has been done as described by Fujimoto and colleagues. Each 10 nM of ss72-nt, ss731-nt, ds681-nt and full-length mRNA or each 5 ng/μL of whole DNA and total RNA, 100 nM effecter ODN and 2 mM $MgCl_2$, in 1x PBS were heated at 90 °C for denaturing, then chilled on ice for annealing. Next, the target and ODN were combined at 37 °C for 2 min. To subject photoligation, the samples were irradiated by 366 nm UV on ice in 5 min by using a UV-LED irradiation device (Omron). This device can irradiate narrow peak UV. Then, the deamination reaction was performed at 90 °C for 2 h or 37 °C for 2 days. Then, the samples were irradiated by 312 nm UV in 30 min by using UV transilluminator (National Biological Corp.) for photosplitting. After photodeamination protocol, base substitution from C to U was confirmed by PCR followed by restriction fragment length polymorphism (RFLP). In that case of full-length RNA or total RNA, RT-PCR was carried out before RFLP. For cDNA synthesis, full-length RNA or total RNA was used in total volume of 20 μL in the present of 0.5 μg random primer, 0.5 mM dNTPs, 1x first-strand buffer, 5 mM DTT, 2 U RNaseOUT (40 U/μL) and 10 U SuperScript III reverse transcriptase (200 U/μL) (Invitrogen). The reaction was incubated for 1 h at 50 °C, and the reaction was deactivated by heating at 50 °C for 30 min.

2.2.3. RFLP (Restriction Fragment Length Polymorphism)

Base substitution from C to U was confirmed by PCR followed by restriction fragment length polymorphism (RFLP). Briefly, the same sequence as the trail synthetic ss72-nt target was amplified by PCR after photodeamination processes. The couple primer sequences were hmtDNA-ATP6_8957-F: GGCCTGCAGTAATGTTAGCG and hmtDNA-ATP6_9028-R: TCGAAACCATCAGCCTACTC (Operon Biotechnologies). The PCR mixture contained 50 ng of target, 2 mM $MgCl_2$, 0.1 mM dNTPs, 1x Ex Taq Buffer, 0.25 U of Ex Taq (Takara Bio) and 2 pmol of each primer in 12.5 μL of total reaction mixture. The PCR conditions were initially denatured at 94 °C for 5 min, followed by a cycle of denaturing at 94 °C for 30 sec, annealing at 54 °C for 30 sec and extension at 72 °C for 10 sec. 40 cycles of amplification were performed. The PCR reactions were completed by 1 min extension at 72 °C.

Amplified samples were subjected to RFLP analysis by using *MvaI* enzyme (Takara Bio). The digestion mixture contained 1 μg of amplified sample, 10 U MvaI, 1x buffer K in 25μL of total reaction mixture. Reaction mixture was incubated at 37 °C in 2 h. *MvaI* could cut CCTGG but not CCCGG. This means wild type sequence could be cut, whereas mutated sequence could not by the restriction enzyme (Fig.2.1). The digestion mixtures were electrophoresed in 8% polyacrylamide gels, and stained with SYBR Green I Nucleic Acid

Gel Staining (Cambrex). The images were visualized by using LAS-3000 (Fujifilm). Densitometric analysis was performed by using Multi Gauge ver3.0 software (Fujifilm).

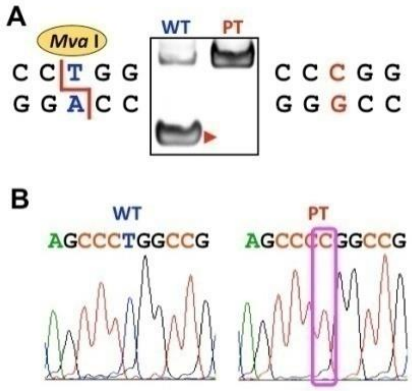

Figure 2.1: Confirmation of T8993C mutation in the patient. *MvaI* could digest wild-type, but it could not digest T8993C mutation of Leigh syndrome patient. The result was confirmed by RFLP (A), and Sanger sequencing analysis, B. WT; wild type, PT; patient.

2.3. RESULTS

2.3.1. Site-directed deamination toward synthetic single strand 72nt-target.

As described before, the efficiency of the base substitution was almost 100% when the responsive ODN and a short 20-mer target were used *in vitro* [16]. The new target must be designed much longer than 20-mer. Therefore, we made a synthetic target which was elongated to 72-mer ODN (synthetic ss72-nt). The synthetic sequences were based on

ATPase6 gene, and it must contain a part of sequence of T8993C mutated ATPase6 which was found in one Leigh syndrome patient.

For effecters of deamination, we designed and synthesized five different ODNs (ODN1 to 5) as shown in Table 2.1 for the trial experiment of site-directed photochemical deamination. They have the same a photoresponsive nucleobase (^{CV}U) in 5'-terminus, but they have different length of complementary part sequences or different length of hairpin loop.

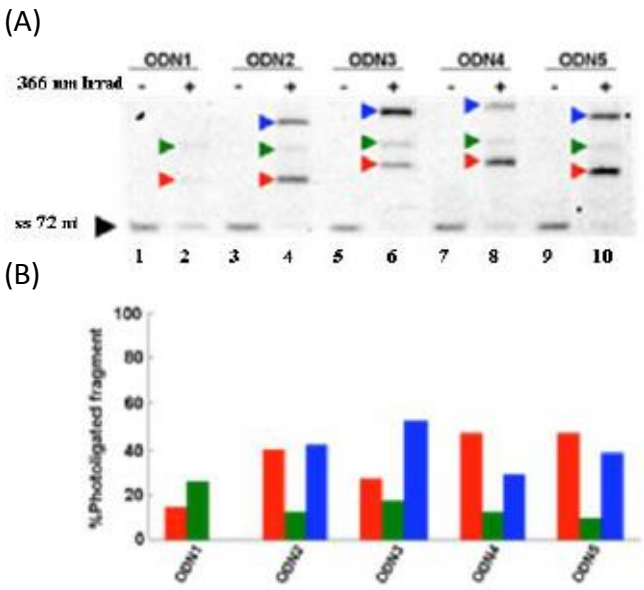

Figure 2.2: Efficiency of photoligation reactions by 5 ODNs and ss72-nt as target at 5 min of 366 nm UV photoirradation. (A) ss72-nt target was subjected to photoligation reaction, then analyzed by denaturing gel polyacrylamide and SYBR green staining. (B) Densitometric analysis of photoligation products from Fig.2.2A.

For photochemical base substitutions, mixtures including 10 nM ss72-nt target, 100 nM effecter ODN and 2 mM $MgCl_2$, in 1x PBS were heated at 90 °C, then chilled on ice, then heating to 37 °C in 2 min for annealing. To subject photoligation, the samples were irradiated by 366 nm UV on ice using a UV-LED irradiation device that can irradiate narrow peak UV. Then, the deamination reaction was performed at 90 °C for 2 h. Then, the samples were irradiated by 312 nm UV using a UV transilluminator for photosplitting. Finally, we confirmed a possibility of photochemical base substitution by using RFLP following PCR. Restored mutation (C>U) must be cut by *MvaI*, therefore, we can observe efficient photochemical deamination by measuring the densitometry of cut bands.

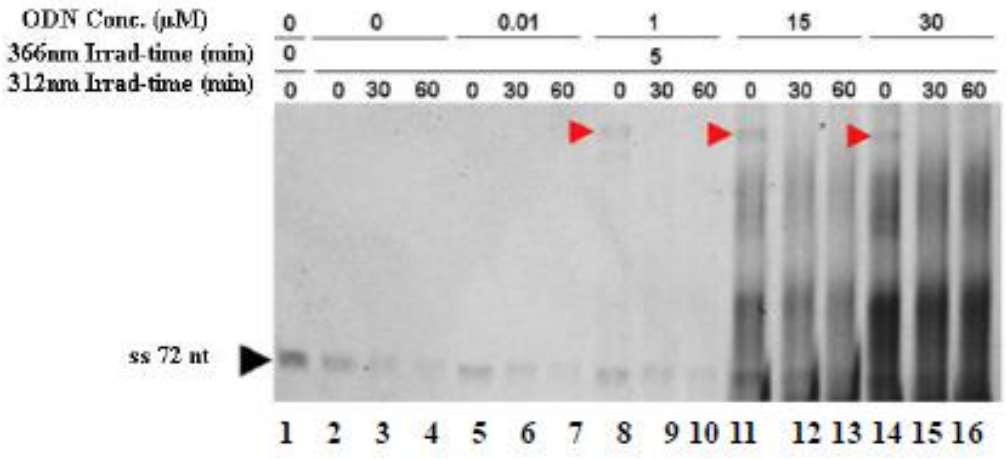

Figure 2.3: Conditions for ss72-nt target treatment. ss72-nt target was subjected to photodeamination, then analyzed by RFLP at the conditions which were 0, 0.01, 1, 15 and 30 μM ODN1 concentration, 0 and 5 min of 366 nm UV radiation and 0, 30 and 60 min of 312 nm UV. The result was analyzed in denaturing gel polyacrylamide and SYBR green staining.

To survey the photoligation efficiency of 5 ODNs with ss72-nt target, the ss72-nt target was subjected to photoligation reactions with ODN 1, 2, 3, 4 and 5, respectively, and the photoligation products were checked by denaturing gel electrophoresis and SYBR green staining. As shown in Fig.2.2, all five ODNs made the photoligation products (Lanes 2, 4, 6, 8 and 10) in comparison with negative controls without ODNs (Lanes 1, 3, 5, 7 and 9), respectively after photo-irradiation.

The efficiency of treatment depends on both the concentration of effecter ODNs and the time of photoligation and photosplitting. Accordingly, we investigated the photochemical reaction with 10 nM ss72-nt target in different conditions of ODN1 concentration and/or time of photoligation and photosplitting to determine the optimum conditions for transition. When ss72-nt target was radiated at 366 nm in absence of ODN1, no photoligation products were observed (Fig.2.3; lanes 1, 2, 3 and 4), but in the presence of ODN1 in 1, 15 and 30 μM, respectively, the expected photoligation products were observed (Fig.2.3; lanes 8, 11 and 14). When ODN1 concentration is 0.01 µM, the photoligation could not be occurred (Fig.2.3; lanes 5, 6 and 7). When photoligation mixture was radiated at 312 nm UV, the photosplitting will be occurred, and the photoligation products will be not presented (Fig.2.3; lanes 9, 10, 12, 13, 15 and 16). Thirty minutes is enough for photosplitting reaction (Fig.2.3; lanes 9, 12, and 15).

From these results, we concluded that optimum conditions for treatment of ss72-nt target were 1 μM ODN1 concentration, 5 min for 366 nm UV irradiation and 30 min for

312 nm UV irradiation. After carrying out these experiments, we found that the most effective ODN is ODN2 among 5 ODNs (Fig.2.4).

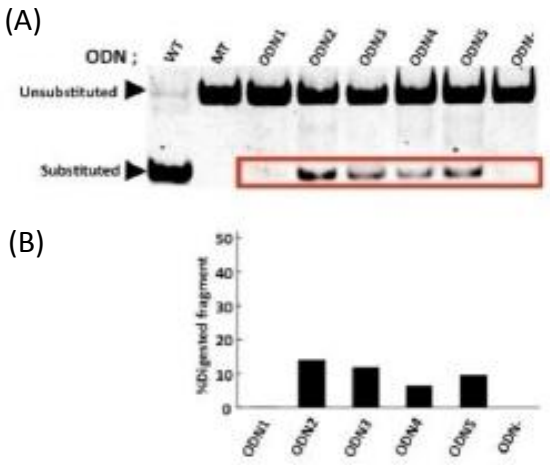

Figure 2.4: Efficiency of site-directed deamination by 5 ODNs and synthetic ss72-nt target. A ss72-nt target was subjected to photochemical deamination, then analyzed by PCR-RFLP. (A) Result of RFLP, WT; wild type, MT; mutant, ODN*; ODN1 to 5 and no ODN. A red box is corresponding bands with digested samples. (B) Densitometric results of base substitutions from Fig.2.4A.

2.3.2. Site-directed deamination toward various targets.

Physiological targets of the effecter ODNs are the mitochondrial DNA and mRNA. Therefore, we prepared series of targets, including ss731-nt, ds681-nt (double strand 681-nt DNA), whole DNA (both purified genome and mitochondrion DNA from the patient's cells), full-length ATPase6 mRNA (813nt) and total RNA (purified from the patient's cells). Then, each 10 nM of ss72-nt, ss731-nt, ds681-nt and full-length mRNA or each 5 ng/μL of whole DNA or total RNA was added to the reaction mixture with 100 nM ODN2 and was

subjected to photochemical deamination, essentially same as described above. As shown in Fig.2.5, photochemical base substitution was succeeded to some of these targets.

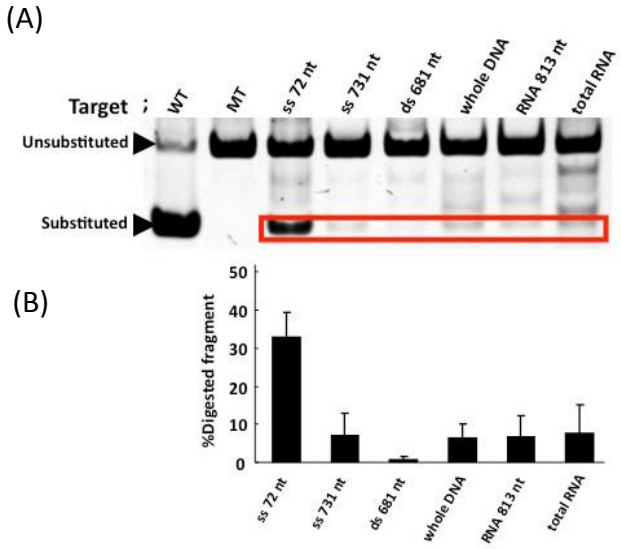

Figure 2.5: Efficiency of site-directed deamination toward various targets. Various targets were subjected to photochemical deamination, then analyzed by RFLP. ODN2 was used as an effecter. (A) Result of RFLP, target was described on the top of each lane. A red box is corresponding bands with digested samples. (B) Densitometric results of base substitutions from Fig.2.5A. MT: mutant.

2.3.3. Site-directed deamination at 37 °C.

In previous experiments, we used 90 °C in the heat treatment for deamination. However, we cannot use non-physiological condition for disease treatment. It is possible that deamination process occurs in low temperature. Therefore, we subjected longer incubation at 37 °C for 48 h instead of 90 °C for 2 h.

Interestingly, the efficiency of the base substitution toward full-length ATPase6 mRNA and total RNA from the patient's cells increased, when the deamination reaction was

performed at 37 °C for 2 days instead of 90 °C for 2 h (Fig.2.6). By repeating experiments, almost 10% of site-directed deamination was observed.

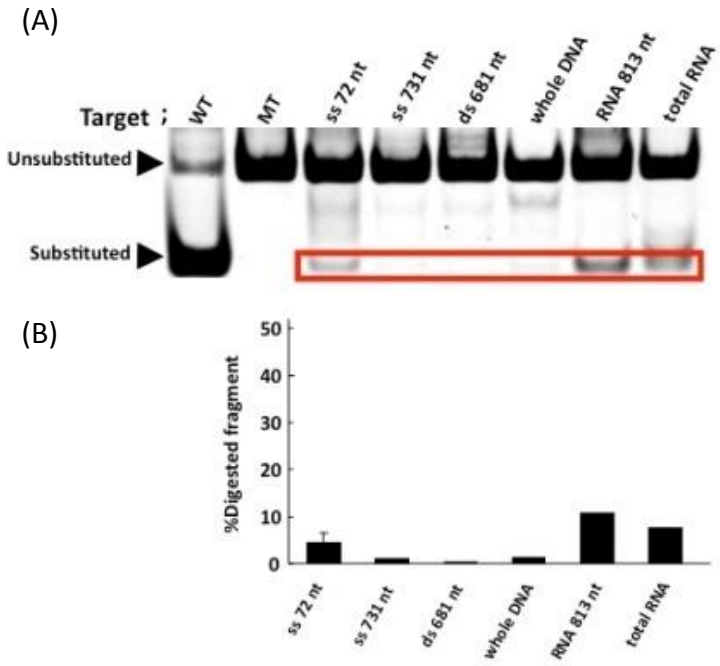

Figure 2.6: Efficiency of site-directed deamination toward various targets at 37 °C. Various targets were subjected to photochemical deamination, then analyzed by RFLP. (A) Result of RFLP, target was described on the top of each lane. A red box is corresponding bands with digested samples. (B) Densitometric results of base substitutions from Fig.2.6A.

2.4 DISCUSSION

Our aim tried to restore genetic code of mutated RNA into “healthy” RNA. In this paper, site-directed photochemical deamination technology was carried out to repair T>C mutation.

Among examined 5 ODNs, ODN2 could convert C to U most effectively (Fig.2.4). As shown in Table 2.1, ODNs having longer complementary sequences of the target seems to work well. This result is reasonable that longer sequences should bind stronger to the target.

Better results were observed when the heat- treatment was performed at 37 °C in 2 days instead of 90 °C in 2h by using RNA as a target (please compare Fig.2.5 and Fig.2.6). It is known that RNA is destroyed quickly in higher temperature. The result might be caused by stabilization of RNA in lower temperature.

We succeeded a sequence-specific photochemical base substitution toward whole DNA and total RNA from patient’s cells used as a target (Fig.2.5 and Fig.2.6). This result suggested the possibility of restoration of mutated full-length mRNA. Because DNA is present as double-stranded form in cells in usual, RNA should be target for the site-directed restoration of genetic code. We found that almost 10% of RNA was targeted deamination *in vitro*. It is not efficient enough to treat a genetic disorder. However, we

believe that the site- directed photochemical deamination technology could be improved to develop more efficiently.

2.5 CONCLUSION

In this research, we observed efficient site-directed base-substitution by using photochemical deamination *in vitro*. The C>U substitution means restoration of genetic code in diseases caused T>C point mutations. Therefore, we concluded that photochemical site-directed deamination technology could be useful for novel genetic restoration therapy towards genetic disorders caused T>C point mutations.

2.6 REFERENCES

[1] Leigh D: **Subacute, necrotizing encephalomyelopathy in an infant.** *J Neurol Neurosurg Psychiatry* **1951**, 14:216-221.

[2] Pronicki M, Matyja E, Piekutowska-Abramczuk D, et al. **Light and electron microscopy characteristics of the muscle of patients with SURF1 gene mutations associated with Leigh syndrome.** *J Clin Pathol* **2008**, 61: 460-6.

[3] Debray FG, Lambert M, Lortie A, Vanasse M, Mitchell GA: **Long-term outcome of Leigh syndrome caused by the NARP-T8993C mtDNA mutation.** *Am J Med Genet [A]* **2007**, 143: 2046-2051.

[4] Cooper MP, Qu L, Rohas LM, et al. **Defects in energy homeostasis in Leigh syndrome French Canadian variant through PGC-1alpha/ LRP130 complex.** *Genes Dev* **2006**, 20: 2996-3009.

[5] Rahman S, Blok RB, Dahl HH, et al. **Leigh syndrome: Clinical features and biochemical and DNA abnormalities.** *Ann Neurol* **1996**, 39: 343-351.

[6] Ostergaard E, Hansen FJ, Sorensen N, et al. **Mitochondrial encephalomyopathy with elevated methylmalonic acid is caused by SUCLA2 mutations.** *Brain* **2007**, 130: 853-61.

[7] Arii J, Tanabe Y: **Leigh syndrome: Serial MR imaging and clinical follow-up.** *AJNR* **2000**, 21: 1502-1509.

[8] Chol M, Lebon S, Bénit P, et al. **The mitochondrial DNA G13513A MELAS mutation in the NADH dehydrogenase 5 gene is a frequent cause of Leigh-like syndrome with isolated complex I deficiency.** *J Med Genet* **2003**, 40: 188-191.

[9] Wortmann S, Rodenburg RJ, Huizing M, et al. **Association of 3-methylglutaconic aciduria with sensori-neural deafness, encephalopathy, and Leigh-like syndrome (MEGDEL association) in four patients with a disorder of the oxidative phosphorylation.** *Mol Genet Metab* **2006**, 88: 47-52.

[10] Jareño NM, Fernández-Mayoralas DM, Silvestre CP, Cortés BM, Pérez MU, Campos-Castelló J: **3-Methylglutaconic aciduria type 4 manifesting as Leigh syndrome in 2 siblings.** *J Child Neurol* **2007**, 22: 218-221.

[11] Di Rocco M, Caruso U, Moroni I, et al. **3-Methylglutaconic aciduria and hypermethioninaemia in a child with clinical and neuroradiological findings of Leigh disease.** *J Inherit Metab Dis* **1999**, 22: 593-598.

[12] Carelli V, Baracca A, Barogi S, et al. **Biochemical-clinical correlation in patients with different loads of the mitochondrial DNA T8993G mutation.** *Arch Neurol* **2002**, 59: 264-270.

[13] Uziel G, Moroni I, Lamantea E, et al. **Mitochondrial disease associated with the T8993G mutation of the mitochondrial ATPase 6 gene: A clinical, biochemical, and molecular study in six families.** *J Neurol Neurosurg Psychiatry* **1997**, 63: 16-22.

[14] Wong LJ: **Pathogenic mitochondrial DNA mutations in protein-coding genes.** *Muscle Nerve* **2007**, 36: 279-293.

[15] Piao YS, Tang GC, Yang H, Lu DH: **Clinico-neuropathological study of a Chinese case of familial adult Leigh syndrome.** *Neuropathology* **2006**, 26: 218-221.

[16] Fujimoto K, Matsuda S, Yoshimura Y, Matsumura T, Hayashi M, Saito I: **Site-specific transition of cytosine to uracil via reversible DNA photoligation**. *ChemComm.* **2006**, 3223-3225.

CHAPTER 3: CHANGE FROM BLUE FLUORESCENT PROTEIN TO GREEN FLUORESCENT PROTEIN BY CHEMICAL RNA EDITING AS NOVEL STRATEGY IN GENETIC RESTORATION

3.1. INTRODUCTION

In chapter 2, a mitochondrial DNA T8993C mutation of Leigh syndrome patient was used as model. But after further cell studies (the data was not showed in here), we recognized that the Leigh syndrome patient's cells were not well living, slowly growing, and another harmful future of these cells was difficult to absorb the exogenous ODNs, the new model was necessary. Blue fluorescent protein (BFP), a derivate of green fluorescent protein (GFP) was suggested as new model. GFP was firstly reported by Shimomura in 1962 from *Aequorea* jellyfish [1], and it quickly became popular in molecular biology for studying gene expression, protein folding, and trafficking [2]. It was commonly used in molecular biology, medicine, and cell biology because GFP protein is auto-fluorescence, and no specific enzymes or energy are needed [3, 4]. GFP molecule contains 11-stranded β-barrel. 11-stranded β-barrel make the wall of cylinder. One α-helix runs up the axis of the cylinder, and the chromophore is attached to the α-helix in the center of the cylinder [2]. BFP differs from GFP by a single nucleotide; a C-to-T change at position 199 transforms the BFP gene into the GFP gene. Because of their sequence characteristics, BFP and GFP are highly valuable models for *in vitro* studies on artificial RNA editing. In terms of chemical structure, when deamination reverses the amino group of cytidine at the fourth position

in the pyrimidine ring to a ketone group, the base converts into uridine (Fig. 3.1A), which in DNA is naturally recognized as thymidine. Therefore, the nt-199 conversion of cytidine to uridine changes the BFP sequence into the GFP sequence.

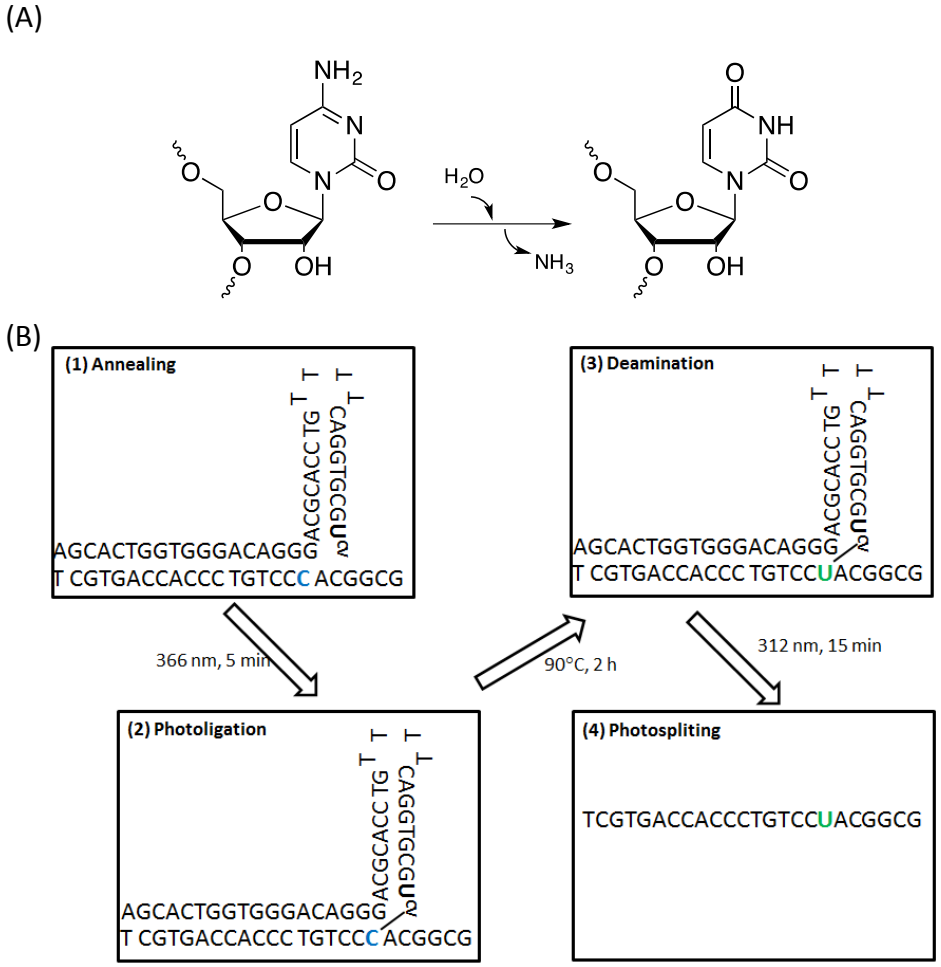

Figure 3.1: Schematic representation of artificial transition. (A) Deamination of cytidine to uridine [5]. (B) The steps of artificial transition. (1) A responsive ODN is annealed with the test sequence that includes a target C. (2) Photoirradiation is performed to photoligate the 5′-^{CV}U with the target. (3) Heat-treatment is used to deaminate an amino residue in the target sequence. (4) After photosplitting of the ODN, site-directed base-transition is completed [6].

In our overall strategy, we used UVA (366 nm) for photoligation and narrow-band UVB (312 nm) for photosplitting. UVA is a major sunlight component that does not cause mutations, and UVB is common used for treating psoriasis and other skin diseases. Although UVB has been related to skin carcinogenesis, several studies have shown that narrow-band UVB phototherapy (311-312 nm UV) does not typically increase skin-cancer risk, and this treatment has thus far been assessed to be very safe [7].

In this study, we designed and studied three 5'-^{CV}U-ODNs. The photo-crosslinking efficiency for C-to-U transition was evaluated using the single stranded 100-nt (ss100-nt) BFP or full-length BFP mRNA targets. Our results showed that substantial amounts of target-base-substituted fragments were successfully generated *in vitro* at physiological temperature.

3.2. MATERIALS AND METHODS

3.2.1. Oligonucleotides

All oligonucleotides were synthesized according to conventional amidite chemistry by using an automated DNA synthesizer. As a synthetic target in trial experiments, we used an oligonucleotide from BFP 129–229 (ss100-nt): 5'-ACCCTGAAGTTCATCTGCACCACCGGCAAGCTGCCCGTGCCCTGGCCCACCCTCGTGACCACCCTGTCC**C**ACGGCGTGCAGTGCTTCAGCCGCTACCCCG-3'. The ^{CV}U-containing oligonucleotides were synthesized as reported [6]. The ODN names and sequences are the following: ODNa, 5'-

^{CV}UGCGTGGTTTTCCACGCAGGGACAGGGT-3'; ODNb, 5'-

^{CV}UGCGTGGTTTTCCACGCAGGGACAGGGTGGTCACGA-3'; and ODNc, 5'-

^{CV}UGCGTGGACTTTTGTCCACGCAGGGACAGGGT-3'.

3.2.2. Plasmid construction

We used the pCI-Neo BFP plasmid. The point mutation in the BFP gene was generated in pCI-Neo GFP by using the QuikChange II Site-Directed Mutagenesis kit (Agilent Technologies). The mutation was confirmed by sequencing. The BFP gene was subcloned via *NdeI* and *XhoI* (New England Biolabs) restriction sites into the DHFR control plasmid (New England Biolabs) by replacing the DHFR gene. The ligation product was transformed into *Escherichia coli* DH5α cells, and then the plasmid was purified using the QIAprep Spin Miniprer kit (QIAGEN) and subjected to thermal sequencing by using the Big Dye Terminator v3.1 DNA Sequencing Kit (New England Biolabs). An ABI Prism 3100 Genetic Analyzer (Applied Biosystems 3130xl Genetic Analyzer) was used for capillary electrophoresis. The plasmid was sequenced across the entire promoter and open reading frame (ORF) and the T7 terminator.

3.2.3. Photochemical deamination

Site-directed substitution by deamination was performed as described by Fujimoto and colleague [6]. Initially, the responsive ODN to be converted was annealed to the target site of the gene to be altered. The targeted cytidine was crosslinked with the responsive ODN

by using 366 nm UV (Omron) and then heat-treated. Lastly, the crosslinked nucleotide was cleaved by means of photosplitting (312 nm UV irradiation-National Biological Corp.). In the survey experiments, the target used was a synthetic ss100-nt oligonucleotide of the BFP sequence, and later full-length BFP mRNA derived from *in vitro* transcription was also used as the target.

3.2.4. Confirmation of base substitution

Base substitution from C to U was confirmed by performing PCR followed by RFLP analysis. Briefly, the same sequence as the synthetic ss100-nt target was PCR-amplified after photochemical deamination, and the amplified samples were subjected to RFLP analysis by using the restriction enzyme *BtgI* (New England Biolabs). Lastly, samples were resolved using PAGE, the gels were stained with SYBR Green I (Cambrex), and images were processed using the LAS-3000 imager (Fujifilm).

3.2.5. *In vitro* transcription and translation

All DNA plasmid templates were linearized by means of *Not*I (Takara Bio) digestion and used to synthesize the BFP mRNAs by using T7 RNA polymerase. Full-length mRNAs were synthesized using the T7 MEGAscript kit (New England Biolabs), as recommended by the manufacturers. After incubation at 37 °C for 4 h, reactions were terminated by placing the samples on ice. Next, mRNAs were purified by means of lithium chloride precipitation or phenol: chloroform extraction and isopropanol precipitation in order to eliminate excess

unincorporated free nucleotides. Subsequently, the mRNAs were recovered using ethanol precipitation, resuspended in nuclease-free water, and quantified using a NanoDrop® ND-1000 spectrophotometer (Nano Drop Technologies). Full-length mRNAs were used for site-direct RNA editing or stored at -80 °C until use. To remove all remaining plasmid DNA templates, the reaction was next treated with *TURBODNase* (15 min, 37 °C). Equal amounts of the reaction products were analyzed using SDS-PAGE, and the gels were stained with SYBR Green (Cambrex) and imaged using the LAS-3000 system. For *in vitro* translation, the full-length BFP mRNA was added to components of the PURESYSTEM kit (New England Biolabs) as per the manufacturer's protocol and the mixture was incubated at 37 °C for 4 h. After the synthesis, the results were quantified by means of western-blotting analysis or spectrofluorometry.

3.2.6. Spectrofluorometry

Spectrofluorometric analysis was performed using a 10-mm quartz cell and a Jasco FP-8600 spectrofluorometer, which is equipped with two monochromators that select two wavelengths as excitation and emission (fluorescence) wavelengths. The fluorometric cuvettes were clear on all sides. Excitation and emission wavelengths were set according to the analysis of BFP and GFP excitation and emission wavelengths. A Xenon flash lamp was used as the light source. Data were acquired and analyzed using the standard software supplied by the manufacturer. Fig. 3.7C showed the emission spectra of BFP and

GFP. To obtain an emission (fluorescence) spectrum, a fixed wavelength was used to excite the molecules, and the intensity of the emitted radiation was monitored as a function of wavelength.

3.2.7. Western blotting

Western blotting was performed as described [9]. To detect full-length BFP or GFP, 1 μL of the *in vitro*-translated product was analyzed using 12% SDS-PAGE. Next, a rabbit polyclonal antibody against GFP (GeneTex, 1: 1000) and an anti-rabbit IgG HRP-conjugated antibody (GE Healthcare, 1: 1000) were used as the primary and secondary antibodies to stain GFP and BFP. The immunoblots were then treated with enhanced chemiluminescence reagents (GE Healthcare) and images were analyzed using the LAS-3000 system (Fuji Film).

3.2.8. The Bradford method and a nanodrop® ND-1000 spectrophotometer were used to measure protein concentrations, according to the manufacturer's instructions (Bio-Rad Laboratories).

3.3. RESULTS AND DISSCUSSION

3.3.1. Optimal conditions for site-directed deamination directed toward the ss100-nt target

To distinguish BFP and GFP sequences, we used PCR-restriction fragment length polymorphism (PCR-RFLP). *BtgI*, a restriction enzyme that can digest "CCACGG" in the coding sequence of BFP but not "CTACGG" in GFP, was suitable for assessing the BFP-to-GFP transition (Fig.3.2). The BFP gene is 720-nt long. Firstly, to determine the optimal conditions for site-directed photochemical RNA editing, we designed and synthesized a synthetic 100-mer ODN target (ss100-nt). The synthetic sequence was based on the BFP coding region, and it was included the portion where the sequence differs at position 199 (ss100-nt sequences are listed in Materials and Methods).

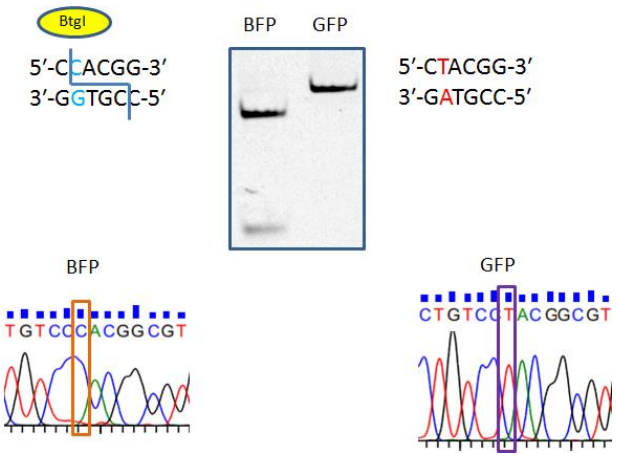

Figure 3.2: Confirmation of a difference in the coding sequences of BFP and GFP. GFP and BFP coding regions differ by a single base pair, which was confirmed using PCR-RFLP analysis.

(A)

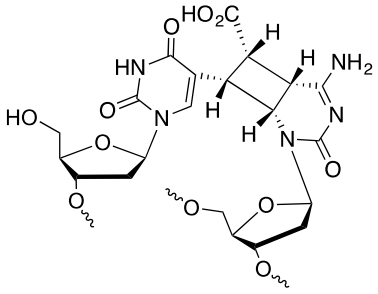

(B)

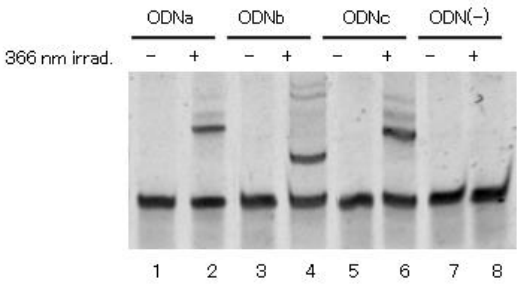

(C)

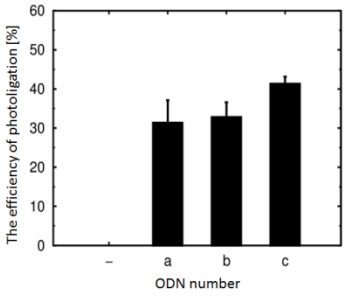

Figure 3.3: Comparison of the efficiency of photoligation between three ODNs and the ss100-nt BFP target after photoirradiation (366 nm) for 10 min. (A) Schematic showing the chemical crosslinking between the ^{CV}U photoreactive group and the targeted C in ss100-nt BFP/ODN heteroduplex [9]. (B) The ss100-nt BFP target was subjected to the photoligation reaction, and the products were resolved using electrophoresis (10% polyacrylamide-7 M urea) and analyzed by means of SYBR Green I staining. (C) Densitometric analysis of the shifted bands shown in (B). The experiment was conducted thrice (n=3), and the efficiency (%) of photoligation in each lane is listed.

Fig.3.3A schematically shows the chemical crosslinking between the ss100-nt BFP target and ^{CV}U-ODNs after photoirradiation. Shifted bands were obtained using all three ODNs tested (Lanes 2, 4, 6; Fig.3.3B), but not without photoirradiation (Negative control; Lanes 1, 3, 5); moreover, when the ss100-nt BFP target was not mixed with ODNs, no shifted bands were observed with and without UV irradiation (Lanes 7, 8). Densitometric analysis revealed that the photoligation efficiency was the highest for ODNc among the three ODNs. After subtraction of the negative control, 40% of ODNc was found to be photoligated with the ss100-nt BFP target (Fig.3.3C).

To examine deamination, we focused on 5′-^{CV}U photoreactive antisense ODNs, because these antisense ODNs have previously been shown to be effective and selective for deamination from cytosine to uridine [6]. We designed and synthesized three ^{CV}U-ODNs, ODNa, ODNb, and ODNc (5′-^{CV}U-ODN nucleotide sequences are shown in Material and methods).

The 5′-^{CV}U-ODNs contain three parts: the sequences of distinct lengths that are complementary to the boundary sequence, the short hairpin loop, and the 5′-terminal photoresponsive nucleobase ^{CV}U. The short hairpin loop of the ^{CV}U photoreactive group allows the target region to be readily accessed and increases the stability of the ODNs. Moreover, the presence of the complementary sequences of the ^{CV}U photoreactive groups increases the binding of the ODNs to the target. The selective crosslinking of photochemical ODNs to the targeted cytosine (photoligation) and the subsequent

photosplitting of the branched ODNs after heat-treatment are two key requirements for efficient, selective C-to-U transition [9].

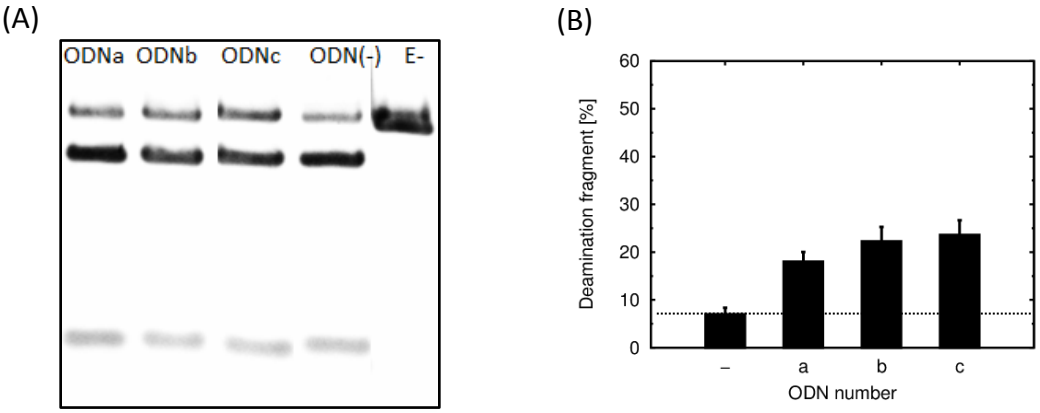

Figure 3.4: Comparison of the efficiency of site-directed deamination between three ODNs and a synthetic ss100-nt BFP target at 90 °C for 2 h. The ss100-nt target was subjected independently to photochemical deamination with three ODNs and then to RFLP analysis. (A) RFLP results: E^-, undigested band; ODN*, ODNa–ODNc; and ODN(-), no ODN. The uppermost bands correspond to undigested samples. (B) Densitometric results of the base substitution shown in (A). The experiment was conducted thrice (n=3), and the results are shown as the efficiency (%) of site-directed deamination in each ODN under a non-physiological temperature.

Photoligation efficiency is a critical factor in successful site-directed RNA editing. To determine the efficiency of photoligation, the ss100-nt target was subjected to photoligation independently with ODNa, ODNb, and ODNc, after which the reaction mixtures were irradiated with 366-nm UV for 10 min at 30 °C. Lastly, the photoligated products were electrophoresed (10% polyacrylamide-7 M urea) under denaturing conditions, the gels were stained with SYBR Green I, and images were processed using a LAS-3000 imager.

The efficiency of site-directed RNA editing depends not only on photoligation efficiency, but also on the efficiency of photosplitting and deamination. For photosplitting, the samples treated with ODNa-ODNc were irradiated with 312 nm UV by using a UV transilluminator. An increase in photosplitting efficiency led to a reduction in the visibility of the shifted bands, and our results showed that 312 nm irradiation performed using a UV transilluminator is a suitable for splitting ^{CV}U photoreactive antisense ODNs. The photosplitting efficiency was the highest for ODNc the three ^{CV}U-bearing ODNs (Fig.3.5). Taken together with previous results, these findings support the conclusion that photoligation under 366 nm UV for 10 min at 30 °C and photosplitting under 312 nm UV for 30 min at room temperature are suitable conditions for chemical site-directed RNA editing.

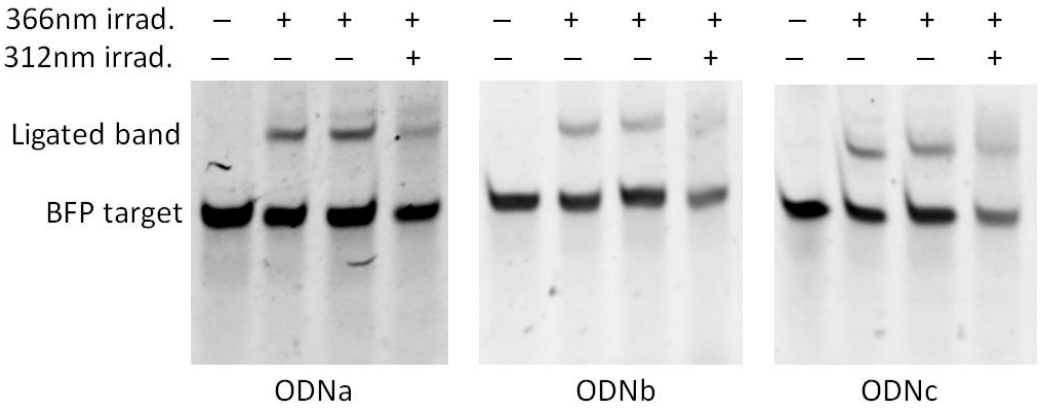

Figure 3.5: Comparison of the efficiency of site-directed chemical RNA editing between three ^{CV}U-ODNs and ss100-nt BFP target. Lanes 1, 5, 9: before ligation; Lanes 2, 6, 10: ligation (366 nm, 10 min); Lanes 3, 7, 11: deamination (90 °C, 2 h); and Lanes 4, 8, 12: photosplitting (312 nm, 30 min).

To perform photochemical base substitutions, mixtures containing 10 nM ss100-nt BFP target, 100 nM effecter ODN, and 2 mM $MgCl_2$ in 1× PBS were heated at 90 °C for denaturation, and then chilled at 37 °C for annealing. First, the samples were irradiated with 366 nm UV at 30 °C by using a UV-LED irradiation device that can generate a narrow UV peak. Next, the deamination reaction was performed at 90 °C for 2 h, after which the samples were irradiated with 312 nm UV by using the UV transilluminator for photosplitting. Lastly, we used PCR-RFLP analysis to monitor potential photochemical base substitution.

Whereas the ss100-nt BFP target should be digested by *BtgI* into two product bands (70- and 30-nt bands), the C199U site-direct transition product should not be digested. In Fig.3.4A, the uppermost band represents successful C199U site-direct transition, and the two product bands (middle and bottom) were generated by *BtgI* digestion. Therefore, we were able to observe and evaluate the efficiency of the photochemical deamination by measuring the density of the remaining undigested bands. The ss100-nt targets are 100mers that were synthesized according to conventional amidite chemistry by using an automated DNA synthesizer. Because the ss100-nt target is very long, ODNs containing synthesis errors could not be removed completely after PAGE and HPLC purification. Therefore, the remaining upper band was observed even when the ODN was used without the deamination procedure, and thus the efficiency of C199U transition was calculated by subtracting the band density of ODN(-) from that of others. Densitometric analysis

(Fig.3.4B) revealed that the C199U transition of ODNc was more efficient than that of the other two tested ODNs. The deamination efficiency of ODNc was 18.4%.

3.3.2. Site-directed deamination directed toward the ss100-nt BFP target under physiological temperature

Disease treatments cannot involve the use of non-physiological conditions, and the 90 °C used for the heat-treatment is exceedingly high. The deamination process could potentially proceed at comparatively occur lower temperatures, and thus we attempted deamination by using a long incubation (10 days) at 37 °C instead of 2 h at 90 °C. The photochemical base substitutions were performed under the same conditions as those in previous experiments, but the deamination reaction was performed at 37 °C for 10 days. After the deamination procedures were completed, PCR-RFLP analysis was used to check for site-directed deamination.

As in previous experiments (Fig.3.4), the uncut band was once again observed even in the case of ODN(-), and we could detect the C199U transition; the presence of the undigested band (Fig.3.6A), and the results of densitometric analysis (Fig.3.6B) showed that efficient C199U transition occurred with all three ODNs. Moreover, as in the case of deamination at 90 °C, site-directed deamination was most efficient in ODNc, and this was estimated to be 6.7%.

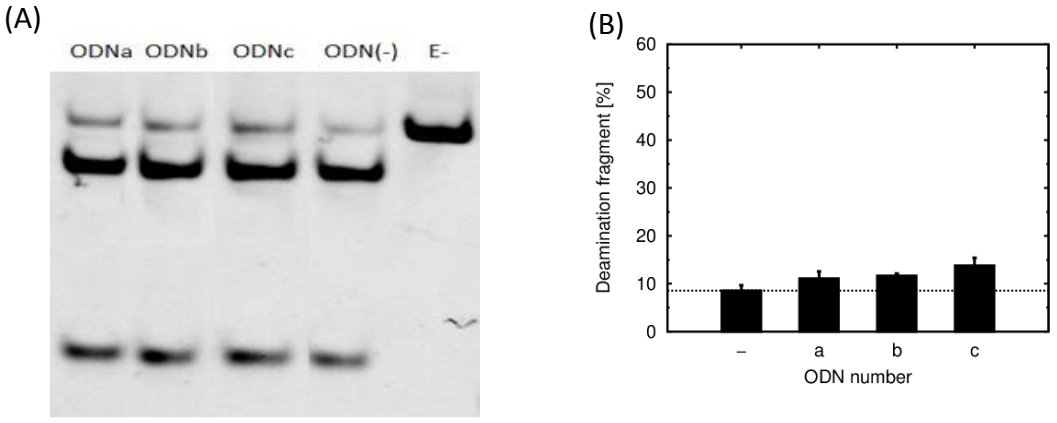

Figure 3.6: Comparison of the efficiency of site-directed deamination between three ODNs and the synthetic ss100-nt BFP target at 37 °C for 10 days. The ss100-nt target was subjected to photochemical deamination and then to RFLP analysis. (A) RFLP results: E^-, undigested band; ODN*, ODNa-ODNc; and ODN(-), no ODN. The uppermost bands correspond to undigested samples. (B) Densitometric results of the base substitution shown in (A). The experiment was conducted five times (n=5), and the efficiency (%) of site-directed deamination measured for each ODN at physiological temperature is shown.

Based on these results, we concluded that at physiological temperature, the ^{CV}U group can function and restore the ss100-nt BFP target by means of C-to-U transition.

3.3.3. Site-directed deamination directed toward full-length BFP mRNA target

In previous experiments, the ss100-nt BFP target was used for optimizing the deamination conditions. However, when treating genetic diseases, the targets are RNAs. Therefore, we next used full-length BFP mRNA BFP as the target; the full-length mRNA of BFP was synthesized *in vitro* and quantified (Materials and methods).

Fig.3.7A shows two strong RNA bands for BFP and GFP, and their 720-nt length suggests that they were full-length, intact mRNAs of BFP and GFP. Next, we used fluorescence-

spectroscopy measurements and confirmed the spectra of *in vitro*-synthesized BFP and GFP. In previous work, the most frequently appearing signals for BFP corresponded to the peak wavelengths of 384 and 448 nm for excitation and emission spectra, respectively, and those for GFP were peak wavelengths of 396 and 508 nm for excitation and emission spectra, respectively [8]. Fig.3.7C shows that the synthesized proteins exhibited compatible peaks.

The *in vitro*-synthesized full-length mRNA of BFP was subjected to photochemical deamination with the three ODNs as described above. Because RNAs could be degraded at 90 °C, deamination procedures were performed at 60 °C for 4 h. For testing the use of physiological conditions, we used 37 °C for 10 days. After photosplitting, the photoreacted samples were used for synthesizing BFP and GFP by using an *in vitro* translation kit according to the manufacturer's protocol. Briefly, 10 μL each of the photoreacted samples were mixed into 50 μL of *in vitro* translation reactions, which were incubated for 4 h at 37 °C. To check for the synthesized proteins, we performed western blotting by using an anti-GFP rabbit polyclonal antibody that can recognize both BFP and GFP (Fig.3.7B); the results showed that full-length BFP and GFP were synthesized.

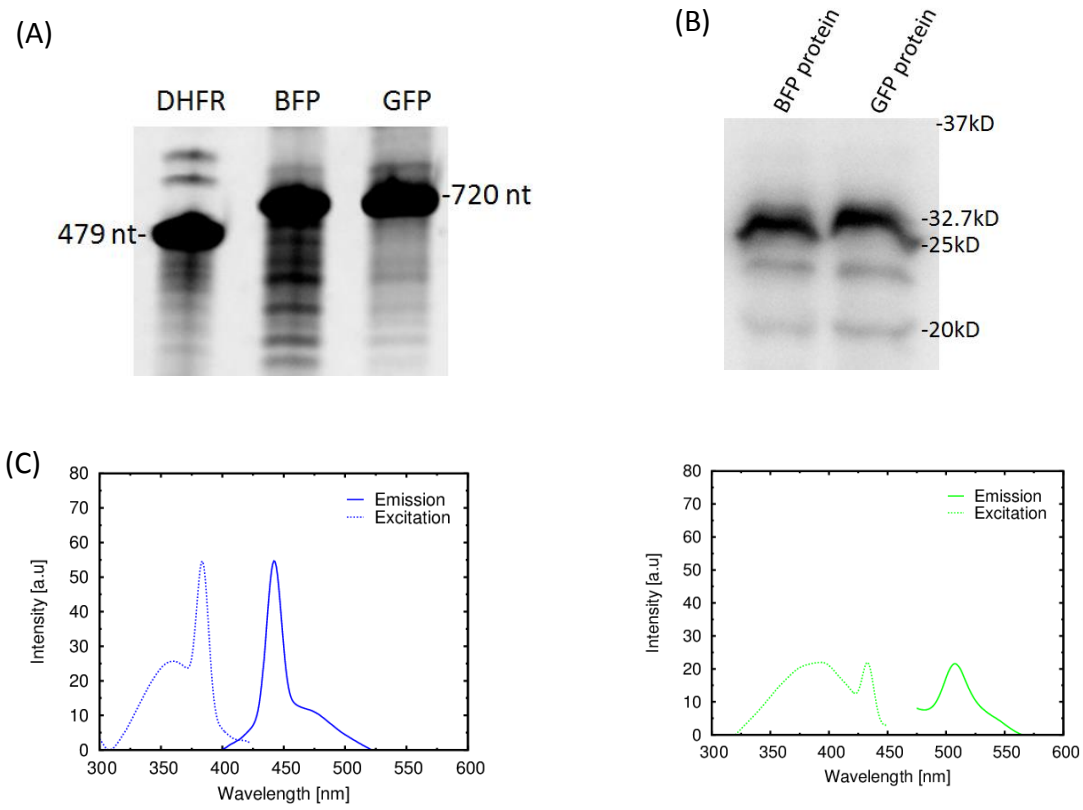

Figure 3.7: *In vitro* transcription of mRNAs of DHFR (dihydrofolate reductase) control, BFP and GFP; and *in vitro* translation of BFP and GFP. (A) The *in vitro* mRNA synthesis was performed using the T7 MEGAscript kit. DHFR mRNA was used as a positive control. Full-length DHFR, BFP, and GFP mRNAs were synthesized successfully. BFP and GFP mRNAs were 720-nt long. (B) Western blotting performed using an anti-GFP rabbit polyclonal antibody that can recognize both GFP and BFP; the images were analyzed using a LAS-3000 system. (C) Spectra of *in vitro*-synthesized BFP and GFP.

We confirmed the synthesis of BFP by using fluorescence spectroscopy (Fig.3.7C). From the fluorescent spectra, we calculated the deamination fraction by determining the ratio of the GFP spectrum area to the sum of the spectrum areas of BFP and GFP. Although the product was translated from the BFP mRNA, ODN(-) did not generate any GFP fluorescence, and the corresponding peak of the GFP signal was observed in site-directed deaminated RNAs (Fig.3.8A). Therefore, we concluded that artificial RNA editing was

induced when we used our procedures at 60 °C. In the non-physiological temperature, transition efficiency was once again the highest for ODNc among the three ODNs, and it was measured to be 16.5% (Fig.3.8A).

Next, we attempted artificial RNA editing under physiological temperature. Our previous results showed that transition efficiency was the highest for ODNc among the three ^{CV}U-containing ODNs (Fig.3.6 and Fig.3.8A). Therefore, we only evaluated the efficiency of deamination of ODNc in the next step.

We performed photochemical base substitutions under the same conditions as those used in previous experiments, but the deamination reaction was at 37 °C for 10 days. To inhibit RNAases, 40 U of an RNase inhibitor was added to 50 μL of reaction mixtures. Fig.3.8B showed that GFP fluorescence was clearly detected when ODNc was used. Spectrofluorometric analysis revealed that ODNc could restore 7.3% of the C-to-U transition (Fig.3.8B).

The signals of the tested samples were detected using fluorescence spectroscopy in a highly reproducible manner, which indicated that the proteins were stable. Therefore, photochemical base substitution could be induced in the synthesized full-length mRNA target at both 60 °C and 37 °C.

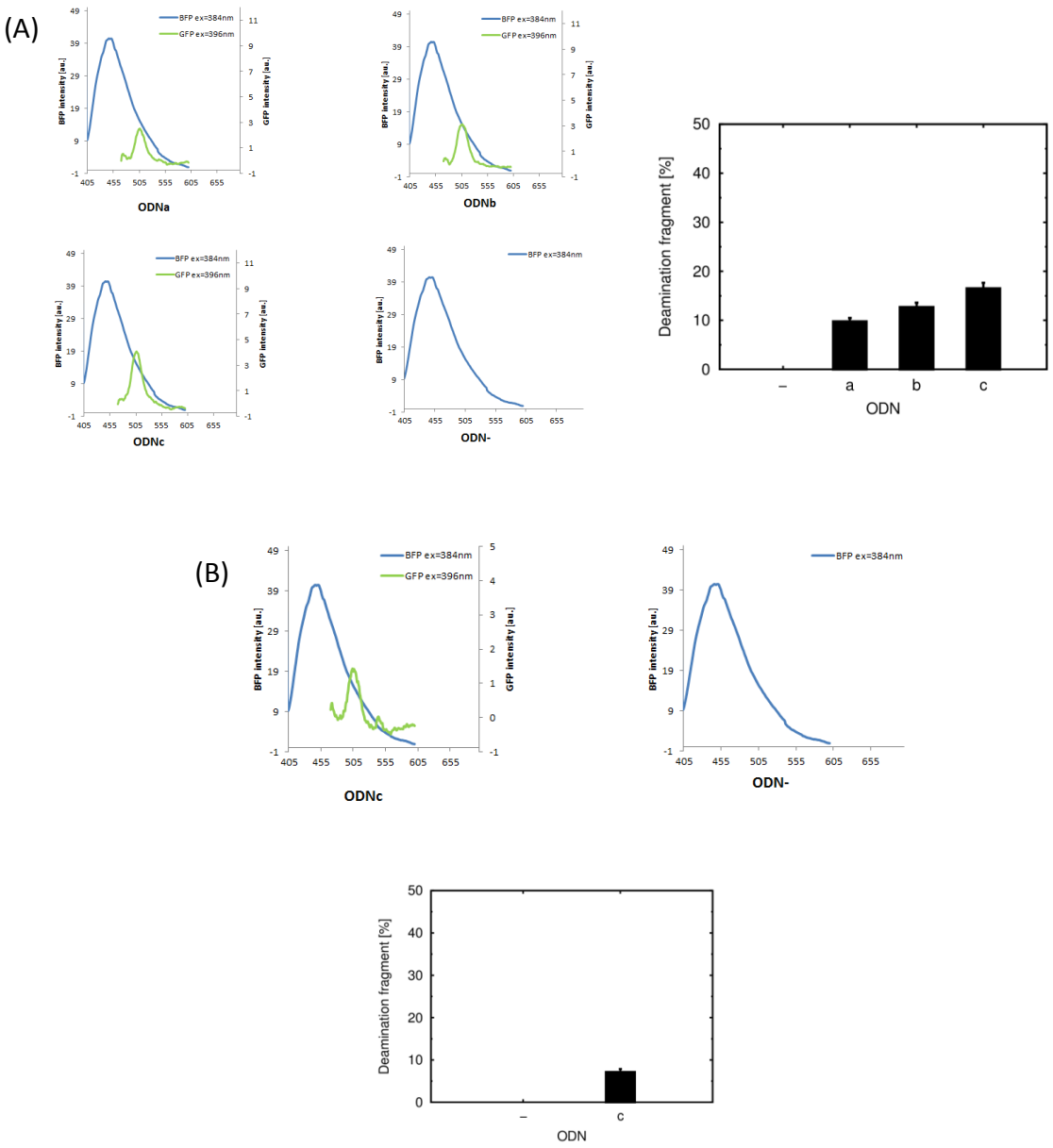

Figure 3.8: Efficiency of site-directed deamination obtained by measurement of BFP and GFP emission spectra. (A) *In vitro*-synthesized full-length BFP mRNA was subjected to photochemical deamination at 60 °C for 4 h, and then the efficiency of deamination was assessed using spectrofluorometric analysis. (B) Efficiency of site-directed deamination obtained by using ODNc together with full-length BFP mRNA as the target at 37 °C for 10 days. ODN*, ODNa-ODNc; and ODN(-), no ODN. The experiment was conducted thrice (n=3), and the results are shown as the efficiency (%) of site-directed deamination in the ODN.

The full-length BFP mRNA was synthesized *in vitro* by using the T7 MEGAscript kit according to the manufacturer's protocol. Briefly, 1 μg each of DHFR-BFP and DHFR-GFP plasmids were linearized using *NotI* restriction enzyme and mixed in 20 μL of the transcription mixtures, which were incubated at 37 °C for 4 h. Plasmid templates were removed by adding 1 μL of TURBODNase (New England Biolabs) into the transcription mixtures. After phenol/chloroform extraction and isopropanol precipitation, *in vitro* transcription products were quantified using a NanoDrop ND-1000 spectrophotometer. The yield from the *in vitro* synthesis of BFP and GFP mRNAs was on average 90 μg/20 μL of total reaction. Next, we performed *in vitro* translation by using the same amount of *in vitro*-synthesized BFP and GFP mRNAs according to the manufacturer's protocol. Briefly, 3 μg of *in vitro* synthesized BFP or GFP mRNA was mixed into 25 μL of *in vitro* translation reactions, which were incubated for 4 h at 37 °C. To calculate the yield of transition GFP, relative fluorescence units were changed to protein mass. First, the total protein in 2 μL of the *in vitro* synthesis reaction and 2 μL of the negative control was quantified using the Bradford protein assay. Because the *in vitro* translation mixtures contain numerous original proteins such as enzymes and proteins of ribosomes, to quantify the synthesized proteins in mixtures, we subtracted total protein of the negative control from that of the synthesized mixture. The results showed that 2 μL of the *in vitro* translation mixture contained approximately 0.5 μg of synthesized proteins and 3 μg of original proteins. Next, we performed western blotting on 3.5 μg of total protein (0.5 μg of synthesized proteins), after which we used densitometric analysis to determine the percentage of BFP or GFP in

the synthesized proteins. The results showed that BFP or GFP constituted 65% of the synthesized proteins. Therefore, 2 μL of the *in vitro* translation mixture contained 0.65 × 0.5 = 0.325 μg of synthesized BFP or GFP.

Based on this finding and the results shown in Fig.7B, we conclude that 0.384 μg of GFP could be generated from 4.8 μg of BFP by using site-directed RNA editing; therefore, after site-directed RNA editing with ODNc under physiological temperature, 1 μg of BFP generates 0.384/4.8 = 0.080 μg (80 ng) of transition GFP (Fig.3.9B).

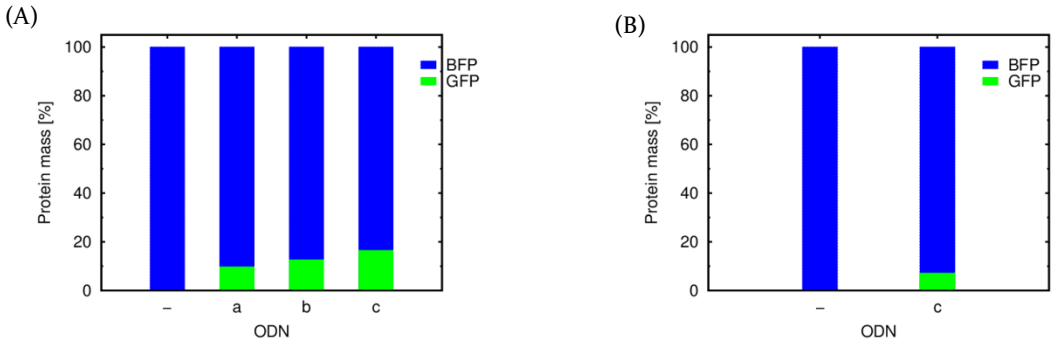

Figure 3.9: Quantification of transition GFP and total original BFP after site-specific, directed RNA editing. (A) RNA editing was performed at 60 °C for 4 h; 180 ng of transition GFP was produced per microgram of original BFP when ODNc was used. (B) RNA editing was performed at 37 °C for 10 days; 80 ng of transition GFP was generated per microgram of original BFP with the use of ODNc.

In summary, we successfully performed *in vitro* transcription and *in vitro* translation. The high reproducibility of the GFP signals, detected using fluorescence measurements, revealed that chemically edited GFP mRNA was generated from the original BFP mRNA after site-direct RNA editing. This indicates that we achieved our aim of restoring the mutated mRNA to a "healthy RNA" under physiological temperature by using photochemical base substitution.

3.4. CONCLUSIONS

In this study, a new method for genetic restoration was established. We successfully performed site-directed photochemical base substitution in synthetic ss100-nt and *in vitro*-synthesized full-length BFP mRNA targets. Among the three tested ^{CV}U-containing ODNs, ODNc exhibited most effective C199U transition under physiological temperature. ODNc contains longer hairpin sequences than do ODNa and ODNb; this appears to work effectively because long sequences increase the stability of ODNs. The C199U transition was more effective in the case of ODNb than in the case of ODNa because the comparatively longer complementary sequence of ODNb will bind more strongly to the target. The relationship between ODN sequences and deamination efficiency is crucial; therefore, we are conducting further studies to identify the optimal sequence for deamination, which we will report soon. We determined that 7.3% of the full-length mRNA was targeted in *in vitro* deamination under physiological temperature. The efficiency is not very high, but this is a first step toward using non-enzymatic, site-directed transition for restoring mutated mRNAs; in future work, this technology will be improved in order to enhance efficiency. This result also suggests the possibility of partially restoring mutated mRNAs. Numerous T>C or G>A point mutations are directly linked to diseases. Thus, repairing a part of a mutated mRNA will partially restore the protein, which should improve the phenotype of patients. We believe that the site-directed photochemical deamination technology could serve as a new method for genetic restoration. Here, we have demonstrated efficient site-directed deamination for genetic restoration *in vitro*.

Because of the requirement of relatively more complex technology, *in vivo* studies that include cultured cells and model animals will be conducted in the near future.

3.5. REFERENCES

[1] Shimomura O, Johnson FH, Saiga Y: **Extraction, purification and properties of aequorin, a bioluminescent protein from the luminous hydromedusan Aequorea.** *J Cell Comp Physiol* **1962**, 59: 223-239.

[2] Tsien RY: **The green fluorescent protein.** *Annu. Rev. Biochem* **1998**, 67: 509-544

[3] Chalfie M, Tu Y, Euskirchen G, Ward WW, Prasher DC: **Green fluorescent protein as a marker for gene expression.** *Science* **1994**, 263(5148): 802-805.

[4] Inouye S, Tsuji FI: **Aequorea green fluorescent protein: expression of the gene and fluorescent characteristics of the recombinant protein.** *FEBS Letter* **1994**, 341: 277-280.

[5] Vu LT, Ooka Y, Alam S, Suzuki H, Fujimoto K, Tsukahara T: **Chemical RNA editing as a possibility novel therapy for genetic disorders.** *Int. J. Adv. Comput. Sci.* **2012**, 2: 237-241.

[6] Fujimoto K, Matsuda S, Yoshimura Y, Matsumura T, Hayashi M, Saito I: **Site-specific transition of cytosine to uracil via reversible DNA photoligation.** *Chem. Commun. (Camb.)* **2006**, 3223-3225.

[7] Lee E, Koo J, Berger T: **UVB phototherapy and skin cancer risk: a review of the literature.** *Int. J. Dermatol.* **2005**, 44: 355-360.

[8] Wachter RM, King BA, Heim R, Kallio K, Tsien RY, Boxer SG, Remington SJ: **Crystal structure and photodynamic behavior of the blue emission variant Y66H/Y145F of green fluorescent protein.** *Biochemistry* **1997**, 36: 9759-9765.

[9] Hakim NH, Kounishi T, Alam AH, Tsukahara T, Suzuki H: **Alternative splicing of Mef2c promoted by Fox-1 during neural differentiation in P19 cells.** *Genes Cells* **2010**, 15: 255-267.

CHAPTER 4: THE RELATIONSHIPS BETWEEN STRUCTURES AND DEAMINATION EFFICIENCY OF CARBOXYVINYLDEOXYURIDINE ODNs ON CHEMICAL RNA EDITING FOR GENETIC RESTORATION

4.1. INTRODUCTION

The deamination efficiency is strongly depended on ODN sequences, relatively little is known concerning the effect of ODN properties on the interactions between the targeted editing and ^{CV}U-ODNs. Therefore, in this study, we were conducted the experiments to identify the optimal ^{CV}U-containing ODN sequences for chemical deamination. To evaluate the structure-deamination efficiency relationships a series ^{CV}U-containing ODNs were designed and studied. The ^{CV}U-containing ODNs have three parts: the complementary part, the hairpin loop, and the 5'-terminal photoresponsive nucleobase ^{CV}U [1]. These oligodeoxynucleotides covalently were showed they bound with the target DNA strand via a [2+2] photocycloaddition between photoreactive nucleoside and deoxycytidine at a specific position in the target DNA on 366 nm UV irradiation. The selective crosslinking of photochemical ODNs to the targeted cytosine (photoligation) and the subsequent photosplitting of the branched ODNs after heat-treatment are two important requirements for efficient, selective C-to-U transition [1]. We observe that the structural sequence dependent deamination efficiency was very tight *in vitro*. And this study has

important significance to design the suitable, optimum oligodeoxynucleotides (ODNs) for treatment of every T>C or G>A caused diseases by using site-directed transition approach.

Figure 4.1: Sequences and structures of ^{CV}U- containing ODNs. These ODNs were name from ODN1-8. The characteristic of them as listed in Table 4.1.

4.2. MATERIALS AND METHODS

4.2.1. Materials

Eight ^{CV}U-containing ODN sequences were used in the study. They differ in the complementary length and hairpin loop length. The structural sequences and minimum free energies of folding of the ODNs are provided in Table 4.1 and Fig.4.1 All oligonucleotides were synthesized by an automated DNA synthesizer according to the conventional amidite chemistry. An oligonucleotide from BFP 129 to 229 (ss100-nt) was used as synthetic target. ^{CV}U containing oligonucleotides were synthesized as reported previously [1]. Stock solutions at a concentration 100 μM were prepare in nuclease-free water and all stock solutions were diluted further in water as required to preparation solutions of desired concentrations.

4.2.2. Preparation of DHFR-BFP plasmid

The BFP gene was subcloned via the *NdeI* and *XhoI* (New England Biolabs) restriction sites into DHFR control plasmid (New England Biolabs) by replacing the DHFR gene. Ligation product was transformed into *Escherichia coli* DH5α cells. The plasmid was purified by using QIAprep Spin Miniprer kit (Qiagen), then this plasmid was subjected to thermal sequencing by using the Big Dye Terninator v3.1 DNA Sequencing Kit (New England Biolabs). An ABI Prism 3100 Genetic Analyzer (Applied Biosystems 3130xl Genetic

Analyzer) performed the capillary electrophoresis. Plasmid was sequenced overall the promoter, whole open reading frame (ORF), and T7 terminator.

4.2.3. Photochemical deamination

The site-directed substitution by deamination has previously done as described by Fujimoto and colleagues [1]. At first, the responsive ^{CV}U-containing ODN was annealed to the target site of the target gene. The target cytidine was cross-linked with the responsive ODN by 366 nm UV irradiation (Omron), then received heat-treatment. Finally, the cross-linked nucleotide is cleaved by the photospliting operation (UV radiation; 312 nm UV). In this study, a synthetic ss100-nt oligonucleotide of blue fluorescent protein (BFP) sequence continued to be use as target. Then, full-length mRNA BFP derived from *in vitro* transcription was also used as target.

4.2.4. Restriction fragment length polymorphism (PCR-RFLP)

Base substitution from C to U was confirmed by PCR followed by restriction fragment length polymorphism (RFLP). Briefly, the same sequence as the synthetic ss100-nt target was amplified by PCR after photodeamination protocol. Amplified samples were subjected to RFLP analysis by using *BtgI* enzyme. *BtgI* (New England Biolabs) could digest CCACGG sequences but not CTACGG sequences. This means that BFP coding sequence was

digested but changed GFP coding sequence is undigested by *BtgI* enzyme as shown in Chapter 3.

4.2.5. *In vitro* transcription and translation

All DNA plasmid templates were linearized by *NotI* (Takara Clontech) digestion, and they were used to synthesize the BFP mRNAs by using T7 RNA polymerase. Full-length mRNAs were synthesized by the T7 MEGAscript kit (New England Biolabs) as recommended by the manufacturers. After incubation at 37 °C for 4 h, mRNAs were further purified on lithium chloride precipitation or phenol/chloroform extraction and isopropanol precipitation to eliminate excess unincorporated free nucleotides. Then, mRNAs were recovered by ethanol precipitation, resuspended in nuclease-free-water, and quantified by using NanoDrop ND-1000 spectrophotometer (Nano Drop Technologies). Full-length mRNA will be used for site-direct RNA editing, or be stored at -80 °C until use. To remove all remained plasmid DNA template, the reaction is subsequently treated with TURBODNase (15 min, 37 °C). Equal amounts of the reaction products were analyzed by sodium dodecyl sulfate-polyacrylamide gel electrophoresis (SDS-PAGE). Gels were stained with SYBR Green II (Takara Bio) and imaged using the LAS-3000 (Fujifilm). For *in vitro* translation, the full-length mRNA BFP is added to the components of PURESYSTEM kit (New England Biolabs) as the company's manual, and the mixture was incubated at 37 °C for 4 h. After

the synthesis, quantitative analyses of the results were carried out using western blot analysis or spectrofluorometor FP8600 (Jasco).

4.2.6. Spectrofluorometry conditions

Spectrofluorometric analysis was performed with the Jasco FP-8600 spectrofluorometer (Jasco). Measurements were carried out with 10 mm quartz cell. It consists of two monochromators, which selects two types of wavelengths as excitation and emission (fluorescence). Fluorometeric cuvettes are clear on all sides. Excitation and emission wavelengths were set according to the analysis of BFP and GFP excitation and emission wavelengths. The most frequently appearing signals for the BFP correspond to the peak wavelengths of 384 nm and 448 nm for the emission and excitation spectra, respectively. Those for the GFP are the peak wavelengths of 396 nm and 508 nm for the emission and excitation spectra, respectively [2]. Xenon flash lamp was used as a light source. Data acquisition and analysis were performed using standard software supplied by the manufacturer. A fixed wavelength was used to excite the molecules, and the intensity of the emitted radiation was monitored as a function of wavelength.

4.2.7. Western blot analysis

Western blotting was performed as previously described [3]. To detect full-length BFP or GFP protein, 1 μL of *in vitro* translated product was analyzed by 12% sodium dodecyl

sulfate polyacrylamide gel electrophoresis (SDS-PAGE). To detect BFP or GFP protein, rabbit polyclonal antibody against GFP (GeneTex, 1: 1000), and anti-rabbit IgG-HRP conjugated antibody (GE Healthcare, 1: 1000) were used as the primary and secondary antibodies, respectively. Membranes were treated using enhanced chemiluminescence (GE Healthcare) and images were analyzed using the LAS-3000 (Fujifilm).

4.2.8. Protein quantification

The Bradford method and NanoDrop ND-1000 spectrophotometer (Nano Drop Technologies) were used to measure the protein concentration, according to the manufacturer's instructions (Bio-Rad Laboratories).

4.3. RESULTS AND DISCUSSION

To evaluate the structure-deamination efficiency relationships a series of the ^{CV}U-containing ODNs were designed, synthesized and studied. We have a series of 7ODNs that the sequences and structures were showed in Fig.4.1 and Table 4.1. As mention in above these ODNs have three parts: the complementary part, the hairpin loop, and the 5'-terminal photoresponsive nucleobase-^{CV}U. The complementary part has important function to anchor and site-direct ODNs with their targets, and the hairpin loop allows ODNs easy access and increase the stability. The chemical structures of 5'-terminal photoresponsive nucleobase-^{CV}U was showed in Chapter 3.

Blue fluorescent protein (BFP), a derivate of green fluorescent protein (GFP), differs from GFP by a single nucleotide, C-to-T transition at position 199 transforms the BFP gene to the GFP gene. To distinguish BFP and GFP sequences, we used PCR-restriction fragment length polymorphism (PCR-RFLP). *BtgI*, a restriction enzyme that can digest CCACGG in the coding sequence of BFP but not CTACGG in GFP, was used for assessing the BFP-to-GFP transition as shown in Chapter 3. To perform photochemical base substitutions, mixtures containing 10 nM ss100-nt BFP target, 100 nM effecter ODN, and 2 mM $MgCl_2$ in 1x PBS were heated at 90 °C for denaturation, and then chilled at 37 °C for annealing. Firstly, the samples were irradiated with 366 nm UV at 30 °C by using a UV-LED irradiation device that can generate a narrow UV peak. Next, the deamination reaction was performed at 90 °C for 2 h or 37 °C in 10 days, after which the samples were irradiated with 312 nm UV by using the UV transilluminator for photosplitting. Lastly, the PCR-RLFP was carried out as Materials and Methods. The ss100-nt BFP target should be digested by *BtgI* into two product bands (70- and 30-nt bands), whereas the C199U site-direct transition product should not be digested. The Figs.4.2, 4.3, 4.5, 4-6, 4.8, 4.9 showed that the uppermost band represented successful C199U site-direct transition, and the two product bands (middle and bottom) were generated by *BtgI* digestion. Therefore, we were able to observe and evaluate the efficiency of the photochemical deamination by measuring the density of the remaining undigested bands by using PAGE and densitometric analysis.

Because physiological target of effector ODNs was mRNA, the *in vitro* full-length mRNA BFP was synthesized by *in vitro* transcription reaction as shown details in the Materials and Methods. Briefly, DHFR-BFP plasmid was linearized by *NotI*, and after the purification, the transcription reaction was set up 1 μg of linearized DHFR-BFP, 2 μL of each dNTP, and 2 μL of T7 transcription enzyme in 1x reaction buffer, and then the mixture was incubated in 4 h. After the phenol/chloroform extraction, isopropanol precipitation was carried out. The *in vitro* full-length mRNA BFP was suspended in nuclease-free water. The *in vitro* 720-nt full-length BFP was successfully synthesized as shown Chapter 3. To perform photochemical base substitutions, 3 μg of *in vitro* full-length was added to the reaction mixture with 100 nM ODN and was subjected to photochemical deamination, essentially same as described above. Then the deaminated mixtures were subjected to *in vitro* translation reactions as shown in Materials and Methods. To check for the synthesized proteins, western blotting was performed by using an anti-GFP rabbit polyclonal antibody that can recognize both BFP and GFP, and the results showed that full-length BFP and GFP were successfully synthesized as my chapter 3. Lastly, spectrofluorometric analysis was performed with the Jasco FP-8600 spectrofluorometer to assess the BFP-to-GFP transition. We used the most frequently appearing signals for BFP corresponded to the peak wavelengths of 384 and 448 nm for excitation and emission spectra, respectively, and those for GFP were peak wavelengths of 396 and 508 nm for excitation and emission spectra [2], respectively to set up the conditions of spectrofluorometric analysis. We

confirmed the synthesis of BFP by using fluorescence spectroscopy. From the fluorescent spectra, we calculated the deamination fraction by determining the ratio of the GFP spectrum area to the sum of the spectrum areas of BFP and GFP. Although the product was translated from the BFP mRNA, ODN(-) did not generate any GFP fluorescence, and the corresponding peak of the GFP signal was observed in site-directed deaminated RNAs as shown in Chapter 3.

4.3.1. The relationship between the hairpin length of ODNs and deamination efficiency

Because the 5'-terminal photoresponsive nucleobase ^{CV}U part was the same for all ODNs, the optimization of the complementary part length and hairpin loop length became two key factors to increase the deamination efficiency.

To evaluate the structure-deamination efficiency relationships the length of hairpin loop was fixed, whereas the length of complementary part was changed. The lengths of hairpin structure were set from 7, 9 and 11nt, and the lengths of complementary changed from 10 to 22nt. Firstly, ^{CV}U-containing ODNs having the same hairpin loop's length, but the different complementary part were used. In this case, the deamination efficiency depends on the length of complementary part.

The transition was carried out for synthetic ss100-nt BFP at 90 °C in 2 h. The ODN of number 1, 2, 3, and 4 were used and also ODN(-) for the comparison. As seen in Table 4.1,

these ODNs have the same hairpin loop length of 7nt, but different sequence complementary lengths. Their complementary part sequences have 10, 14, 18, 22nt long, respectively.

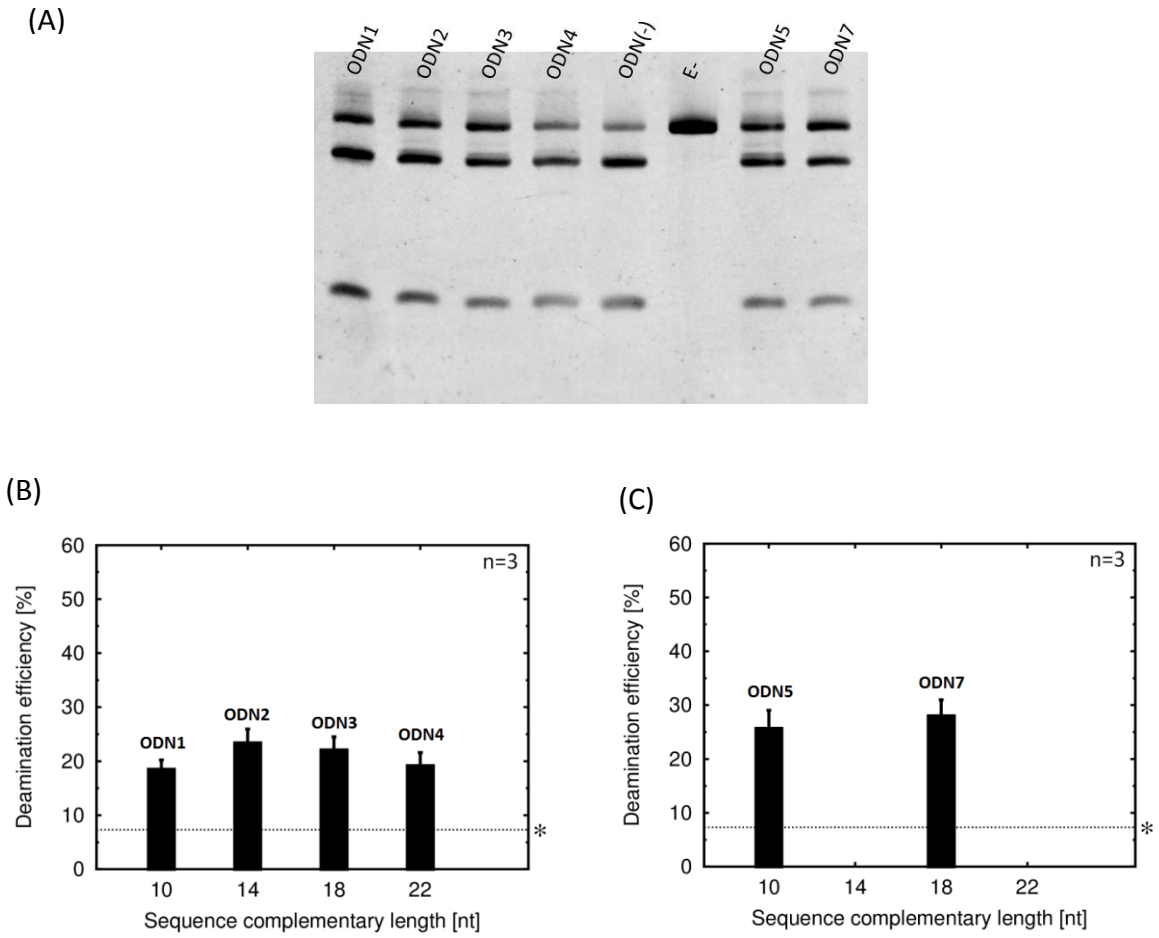

Figure 4.2: The relationship between the complementary part length and the deamination efficiency in non-physiological temperature. (A) The deamination for synthetic ss100-nt BFP template obtained by ODN1, 2, 3 and 4 having the same 7nt hairpin loop lengths, and by ODN5, and 7 having the same 9nt hairpin loop lengths. (B) The densitometric analysis of deamination efficiency for ODN1, 2, 3 and 4 was simultaneously shown with the increase of the complementary part length (C) The same result as (B) was revealed for ODN5 and ODN7. The experiment was conducted thrice (n=3), and the results are shown as the efficiency (%) of site-directed deamination in each ODN under a non-physiological temperature.

Densitometric analysis revealed that with an increase in the sequence complementary length, the deamination efficiency did not change monotonically (Fig.4.2A, and Fig.4.2B). The ss100-nt target has 100mers that was synthesized according to conventional amidite chemistry by using an automated DNA synthesizer. Because the ss100-nt target is very long, ODNs containing synthesis errors could not be removed completely after PAGE and HPLC purification. Therefore, the remaining upper band was observed even when the ODN was used without the deamination procedure, and thus the efficiency of C199U transition was calculated by subtracting the band density of ODN(-) from that of others. From ODN1 to ODN2, the sequence complementary length increased from 10 to 14nt, leading to an increase in the deamination efficiency from 11.2% to 16.1% (these values are obtained after a subtraction by the ODN-). However, from ODN2 to ODN3, the deamination efficiency is almost unchanged even the sequence complementary length increased from 14 to 18nt. For further increase in the sequence complementary length, from 18nt with ODN3 to 22nt with ODN4, the deamination efficiency decreased from 14.8% to about 11.9%. These results indicated that there exists a regime of the sequence complementary length, from 14 to 18nt, in which the deamination efficiency of ODN reached to its optimal value.

Moreover the deamination efficiency also increased slightly from 18.4% with ODN5 to 20.7% with ODN7, which have 9nt hairpin lengths, when the complementary length increases from 10 to 18nt as shown in Fig.4.2A and Fig.4.2.C. The results once time again

confirmed that there exists a regime of the sequence complementary length, from 14 to 18nt, in which the deamination efficiency of ODN reached to its optimal value as above.

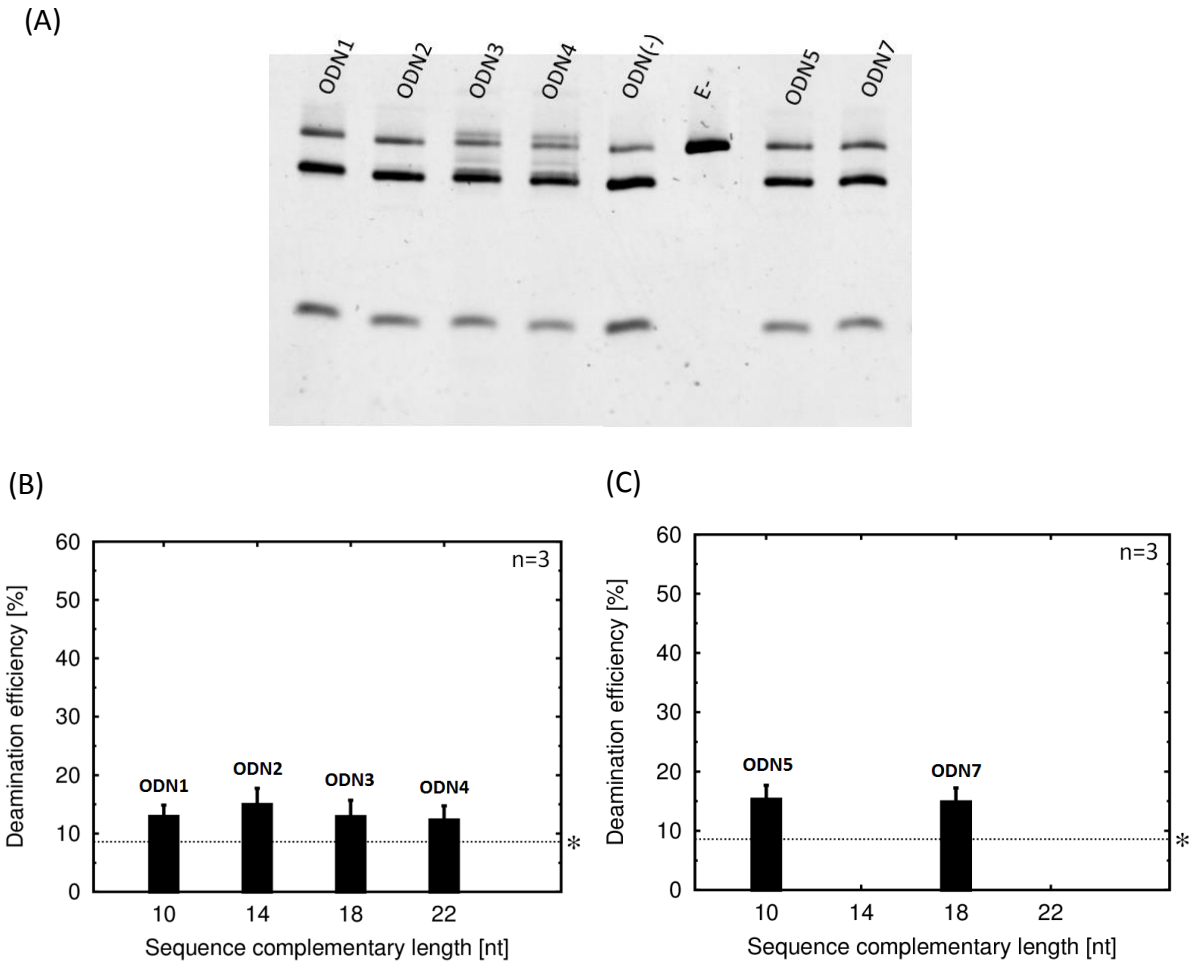

Figure 4.3: The relationship between the complementary part length and the deamination efficiency in physiological temperature. (A) The deamination for synthetic ss100-nt BFP obtained by ODN1, 2, 3 and 4 having the same 7nt hairpin loop lengths, and by ODN5, and ODN7 having the same 9nt hairpin loop lengths. (B) The densitometric analysis of deamination efficiency for ODN1, 2, 3 and 4 was simultaneously shown with the increase of the complementary part length (C) The same result as (B) was revealed for ODN5 and ODN7. The experiment was conducted thrice (n=3), and the results are shown as the efficiency (%) of site-directed deamination in each ODN under a physiological temperature.

In addition, although high deamination efficiencies were not obtained for experiments with the same ODNs at 37 °C, similar tendencies were clearly observed.

(A)

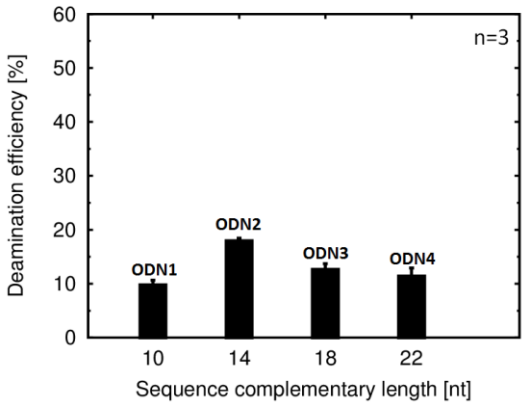

(B)

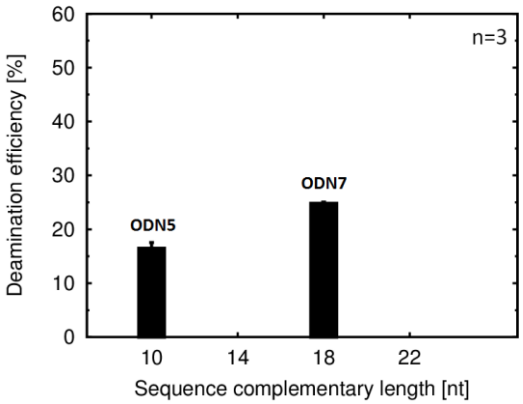

Figure 4.4: The relationship between RNA deamination at non-physiological temperature for *in vitro* full-length mRNA BFP and the various length of complementary part was obtained with (A) ODN1, 2, 3, and 4 having the same 7nt hairpin loop lengths, and with (B) ODN5 and ODN7 having the same 9nt hairpin loop lengths. The experiment was conducted thrice (n=3), and the results are shown as the efficiency (%) of site-directed deamination in each ODN under a non-physiological temperature.

Same as non-physiological experiments above, the ss100-nt target is 100mers that was synthesized according to conventional amidite chemistry by using an automated DNA

synthesizer. Because the ss100-nt target is very long, ODNs containing synthesis errors could not be removed completely after PAGE and HPLC purification. Therefore, the remaining upper band was observed even when the ODN was used without the deamination procedure, and thus the efficiency of C199U transition was calculated by subtracting the band density of ODN(-) from that of others. As seen in Fig.4.3A and B, the deamination increased from 4.3% with ODN1 to 6.4% with ODN2 when the complementary length increased from 10 to 14nt, then decreased from 6.4% (ODN2) to 4.3% (ODN3) with an increase of the complementary length from 14 to 22nt, and continuously decreases to 3.7% with a further increase in the complementary length up to 22nt with ODN4. Hence, the experiment results obtained by using synthetic ss100-nt at both 90 °C and 37 °C showed that the deamination efficiency reached to its maximum value when the complementary length is slightly larger than 14nt (Fig.4.2 and Fig.4.3).

Next, the full-length mRNA BFP was used as target and the detail experiments were shown above and the Materials and Methods. We carried out the experiments with RNA for the same ODNs at 60 °C, and the results were shown in Fig.4.4A. The result revealed that the RNA deamination efficiency increased from 9.8% with ODN1 to more than 18% with ODN2 when the complementary length increased from 10 to 14nt. However, when the complementary length increased from 14 to 18nt, the deamination efficiency decreased from 18% (ODN2) to 12.7% (ODN3). The decrease of the deamination efficiency continued, from 12% with ODN3 to 11.4% with ODN4, with further increases of the

complementary length increases from 18 to 22nt (Fig.4.4A). In that case of ODN5 and ODN7, the result revealed that the RNA deamination efficiency increased from 16.5% with ODN5 to more than 24.8% with ODN7 when the complementary length increased from 10 to 18nt (Fig.4.4B). These results revealed that the dependence of the RNA deamination efficiency at 60 °C on the complementary length, and also implied that the efficiency should reach to its optimal value when the complementary length is slightly larger than 14nt, being consistent with the experimental data for the same ODNs (the first for ODN1, 2, 3, and 4, and the second for ODN5 and 7) with ss100-nt BFP discussed before. The consistence between experiments at different temperatures and also with different templates allows us to conclude that the deamination efficiency depends strongly on the sequence complementary length. The deamination efficiency reached to its optimal value when the complementary length may be equal to 15nt.

4.3.2. The relationship between the complementary length of ODNs and deamination efficiency

Furthermore, in order to investigate the effects of the hairpin length to the deamination efficiency, we carried out experiments with synthetic ss100-nt BFP at 90 °C and 37 °C for ODN1, ODN5, and ODN6. These ODNs have the same sequence complementary length of 10nt, but different hairpin loop lengths. These hairpin loop length are 7, 9, 11nt respectively.

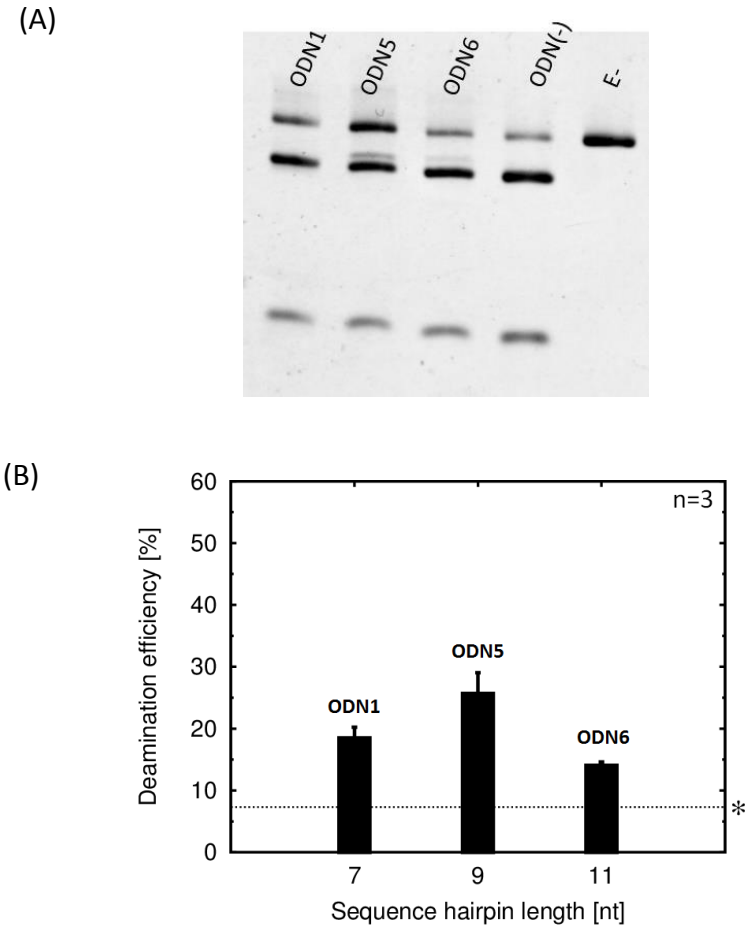

Figure 4.5: The relationship between the hairpin loop length and the deamination efficiency in non-physiological temperature. The deamination for synthetic ss100-nt obtained by ODN1, 5 and 6 having the same 10 nt complementary part lengths. (A) RFLP results: E-, undigested band; (B) Densitometric results of the base substitution shown in A. The experiment was conducted thrice (n=3), and the results are shown as the efficiency (%) of site-directed deamination in each ODN under a non-physiological temperature.

At 90 °C deamination, the densitometric results showed that the deamination efficiency increased from 11.2% with ODN1 to 18.4% with ODN5, corresponding to an increase of the hairpin length from 7 to 9nt. However, when the hairpin length increased from 9nt with ODN5 to 11nt with ODN6, the deamination efficiency decreased from 18.4% to 6.8% (Fig.4.5A and B). These results suggested that the hairpin length should be about 9nt, in

which the deamination efficiency reached to its optimal value. All data were subtracted from ODN(-).

(A)

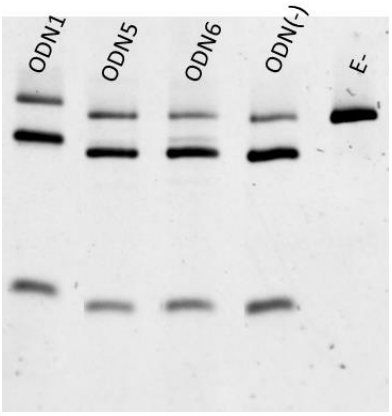

(B)

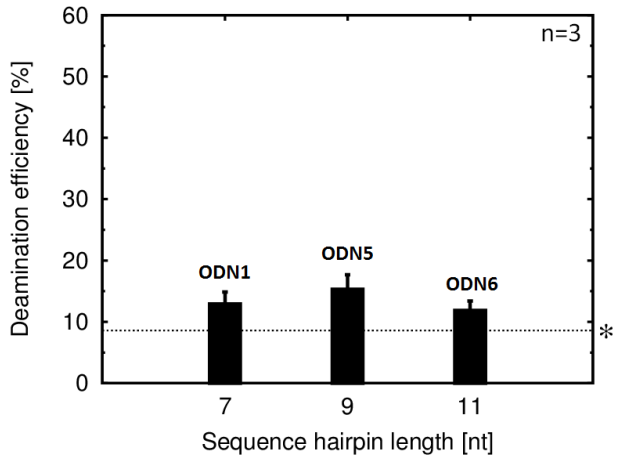

Figure 4.6: The relationship between the hairpin loop length and the deamination efficiency in the physiological temperature. The deamination for synthetic ss100-nt obtained by ODN1, 5 and 6 having the same 10nt complementary part lengths. (A) RFLP results: E-, undigested band; (B) Densitometric results of the base substitution shown in A. The experiment was conducted thrice (n=3), and the results are shown as the efficiency (%) of site-directed deamination in each ODN under a physiological temperature.

Moreover, the same tendencies were also obtained clearly by experiments with the same ODNs at 37 °C. Desitometric analysis showed that the deamination efficiency increased

from 4.3% (ODN1) to 6.7% (ODN5) as the hairpin length increased from 7 to 9nt, but decreased from 6.7% (ODN5) to 3.3% (ODN6) with an increase of the hairpin length from 9 to 11nt (Fig.4.6A and B). All data were subtracted from ODN(-).These results confirmed that the non-enzymatic, chemical deamination efficiency reached to its optimal value with the hairpin length equal to 9nt.

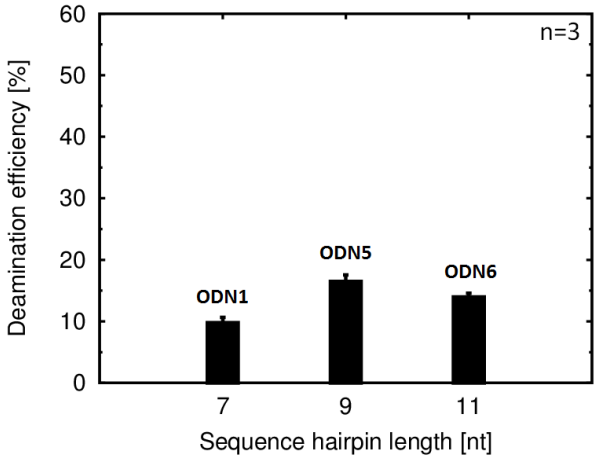

Figure 4.7: The relationship between RNA deamination efficiency at non-physiological temperature (60 °C) for *in vitro* full-length mRNA BFP and the various length of hairpin loop part was obtained by ODN1, 5, and 6 having the same 10nt complementary part lengths. The experiment was conducted thrice (n=3), and the results are shown as the efficiency (%) of site-directed deamination in each ODN under a non-physiological temperature.

In addition to the above discussion about effects of the hairpin length to the chemical transition, we carried out experiments with the same ODN (1, 5, and 6) for full-length mRNA BFP at 60 °C. We can realize a clear dependence of the RNA deamination efficiency on the hairpin length. When the hairpin length increased from 7nt with ODN1 to 9nt with ODN5, the deamination efficiency also increased from 9.8% to 16.5%. However, a further

increase of the hairpin length, from 9nt (ODN 5) to 11nt (ODN 6), leaded to a decrease in the deamination efficiency from 16.5% to 14% (Fig.4.7). These results indicated that the maximum RNA deamination efficiency should be achieved by ODNs with the hairpin length equal to 9nt, confirming the conclusion obtained by experiments with the synthetic ss100-nt BFP as the above.

4.3.3. The optimum hairpin and complementary lengths of ODNs with deamination efficiency

In the first summary, we carried out the experiments with 7 ODNs, which have different sequence complementary lengths or different hairpin lengths, for the synthetic ss100-nt BFP template at 90 °C and 37 °C, and for full-length mRNA BFP at 60 °C. From these experimental results, we showed that there are strong relationship between the deamination efficiency and the sequence complementary length and hairpin loop length. Our investigation showed that the optimal deamination efficiency was achieved with ODNs having a sequence complementary length slightly more than 14nt and a hairpin length of 9nt.

In order to confirm our conclusions on the optimum conditions for the ODNs, we designed, synthesized, and surveyed a new ODN with these conditions, i.e., an ODN has a sequence complementary length of 15nt and a hairpin length of 9nt (ODN8).

(A)

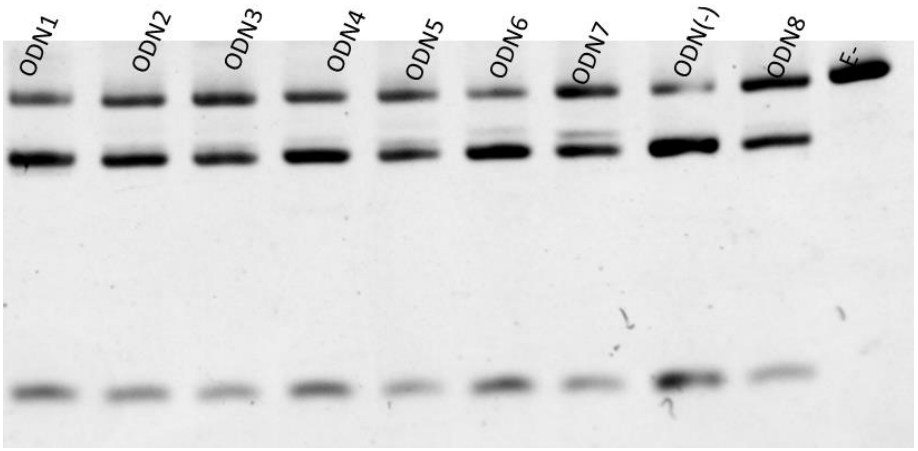

(B)

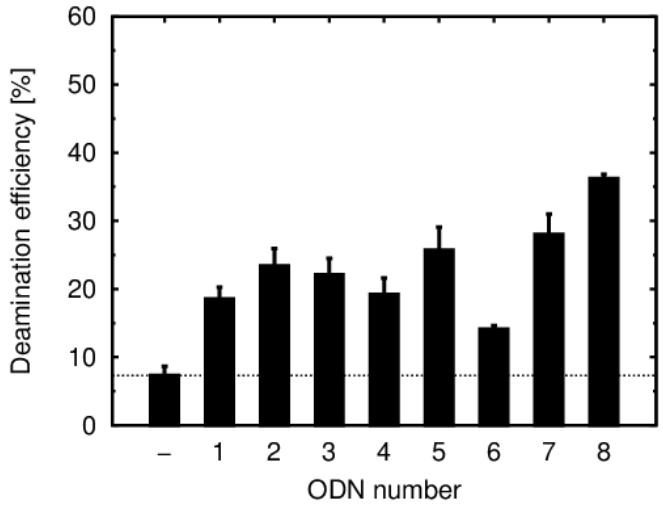

Figure 4.8: The deamination efficiency of ODN8 compared to other ODNs in non-physiological temperature (90 °C). (A) Result of RFLP, target was described on the top of each lane. (B) Densitometric results of base substitutions from Fig.4.8A. The experiment was conducted thrice (n=3), and the results are shown as the efficiency (%) of site-directed deamination in each ODN under a non-physiological temperature.

We carried out the same experiments as the above for the ODN8, and the results are shown in Figs.4.8, 4.9 and 4.10 with data from other ODNs for the comparison. Fig.4.8 and Fig.4.9 showed the experimental results obtained by ODN8 with the synthetic ss100-nt

BFP at 90 °C and 37 °C, the data by other ODNs were also shown simultaneously for the comparison.

(A)

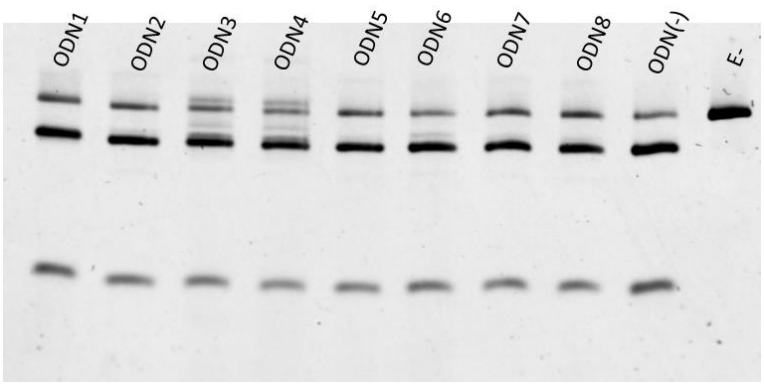

(B)

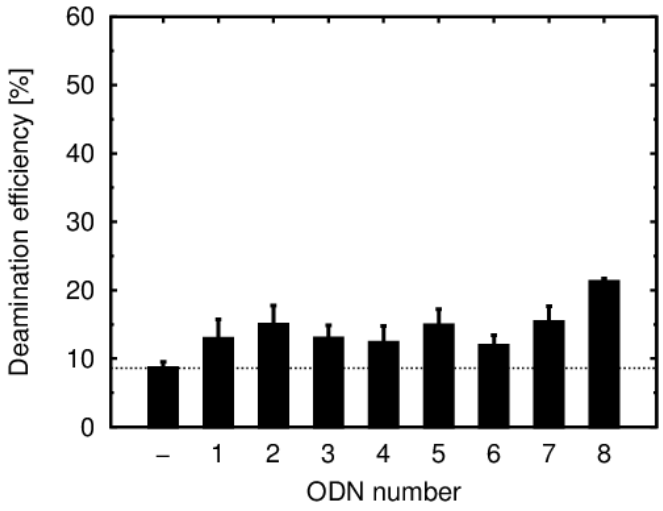

Figure 4.9: The deamination efficiency of ODN8 compared to other ODN in physiological temperature (37 °C). (A) Result of RFLP, target was described on the top of each lane. (B) Densitometric results of base substitutions from Fig.4.9A.The experiment was conducted four (n=4), and the results are shown as the efficiency (%) of site-directed deamination in each ODN under a physiological temperature.

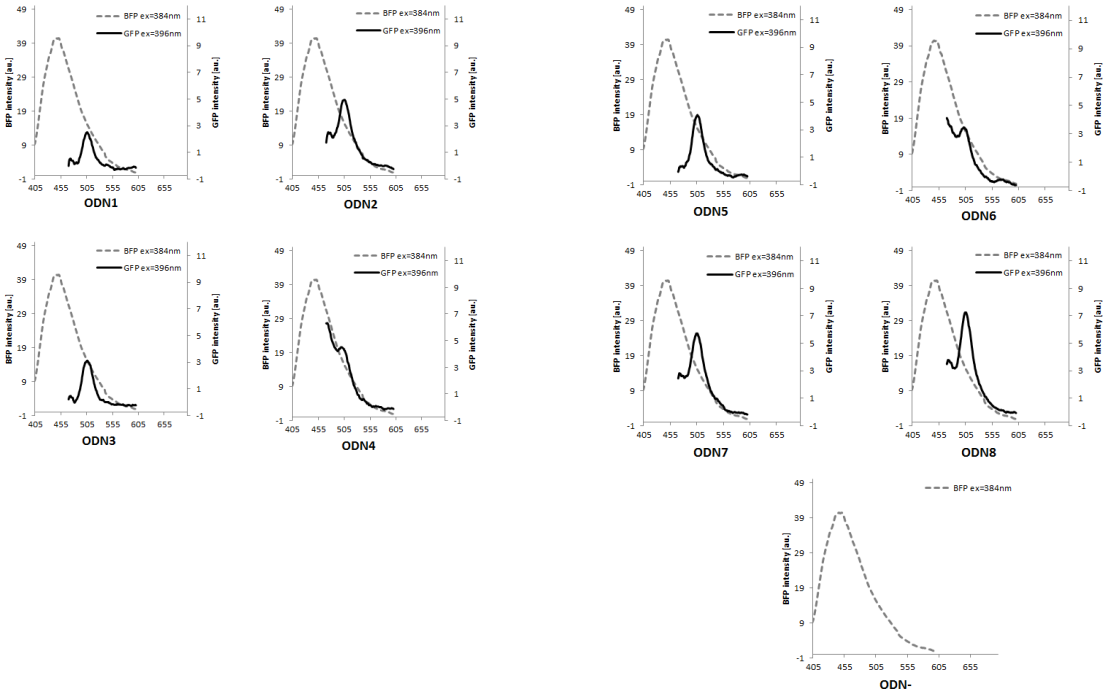

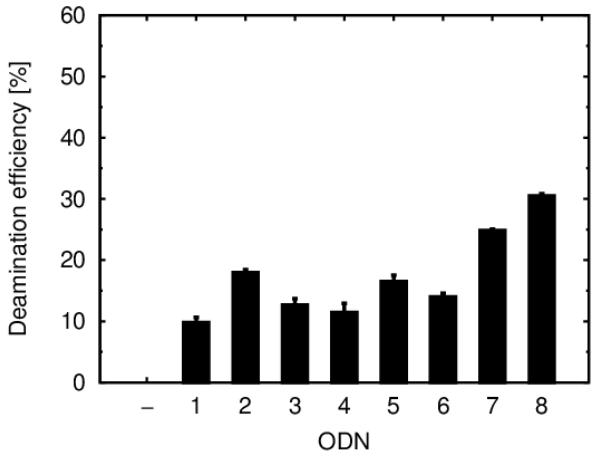

Figure 4.10: The deamination for *in vitro* full-length mRNA BFP obtained by ODN8 comparing to other ^{CV}U-containing ODNs at non-physiological temperature (60 °C). The experiment was conducted thrice (n=3), and the results are shown as the efficiency (%) of site-directed deamination in each ODN under a non-physiological temperature.

We realized that the ODN8 has the highest deamination efficiencies at both 90 °C and 37 °C, as our expectation. The deamination efficiency of ODN8 (after subtraction by ODN-) is 29 % and 12.6 % at 90 °C and 37 °C, respectively. These efficiencies are the highest among 8 ^{CV}U-containing ODNs.

Fig. 4.10 showed the experimental results obtained by ODN8 with the RNA at 60 °C, the data by other ODNs are also shown simultaneously for the comparison. The results showed that the ODN8 has the highest deamination efficiencies among 8 ^{CV}U-containing ODN. The deamination efficiency of ODN8 was 30.5%. We conducted the experiments with ODN8 for the RNA editing at 37 °C. In addition, the same experiments were also carried out for other ODNs, which have high efficiencies in the above experiments, for a comparison. As a result, we used ODN2, 5, and 7 accompanied with the ODN 8 for the RNA editing at 37 °C. Fig.4.11 showed the experimental results obtained by ODN2, 5, 7, and 8 with the *in vitro* full-length BFP mRNA at 37 °C. The result revealed that the ODN8 with optimal structures was the best one, which gave the highest deamination efficiencies. The deamination efficiency of ODN8 was 12.4%.

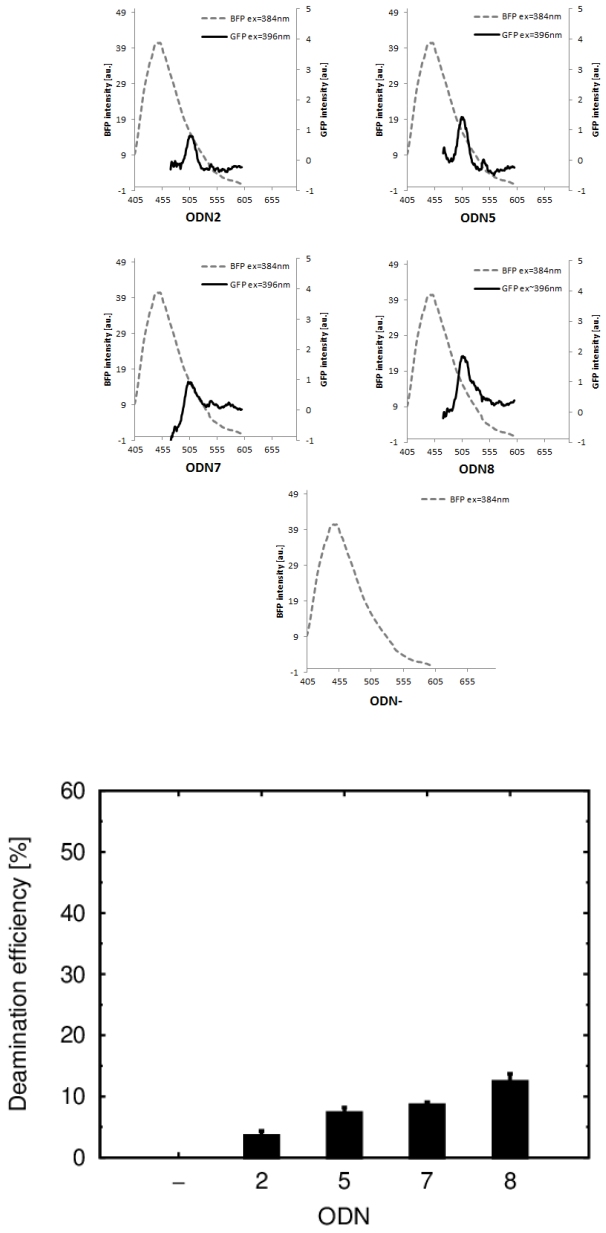

Figure 4.11: The deamination for *in vitro* full-length mRNA BFP obtained by ODN8 comparing to other ^{CV}U-containing ODNs at physiological temperature (37 °C). The experiment was conducted thrice (n=3), and the results are shown as the efficiency (%) of site-directed deamination in each ODN under a non-physiological temperature.

Table 4.1. Sequences of 8 studied ^{CV}U-containing ODNs

ODN name	Complement length (nt)	Hairpin loop length (nt)	Minimum free energy ΔG (kcal/mol) [a]	Melting temperature Tm (°C) [b]
ODN1	10	7	-7.86	85.8
ODN2	14	7	-8.06	71.1
ODN3	18	7	-8.88	72.2
ODN4	22	7	-8.88	72.2
ODN5	10	9	-10.60	89.2
ODN6	10	11	-13.49	91.3
ODN7	18	9	-11.62	76.4
ODN8	15	9	-11.62	76.4

[a] and [b] were calculated and predicted by using 'mFold web server' [4, 5].

4.4. CONCLUSIONS

We have conducted various experiments for 7 ODNs to investigate the dependence of the deamination efficiency on the ODN sequence complementary length and hairpin loop length in order to optimize the ODN structures. The investigation showed the deamination efficiency reached to maximum values with sequence complementary length of 15nt and hairpin loop length of 9nt. As a result, we designed, studied, and obtained the ODN8 with the optimal structure. The optimized ODN increased the deamination efficiencies comparing with the ones obtained by other ODNs without the optimal conditions for 90 °C or 60 °C and 37 °C, respectively for both synthetic ss100-nt BFP and full-length mRNA BFP targets. The deamination efficiency for RNA editing at physiological temperature was about 12.4%, which is considerable. We hope that this studies has significance to design

the suitable, optimum oligodeoxynucleotides (ODNs) for treatment of every T>C or G>A caused diseases by using site-directed transition approach.

4.5. REFERENCES

[1] Fujimoto K, Matsuda S, Yoshimura Y, Matsumura T, Hayashi M, Saito I: **Site-specific transition of cytosine to uracil via reversible DNA photoligation**. *Chem. Commun.* **2006**, 30, 3223-3225.

[2] Wachter RM, King BA, Heim R, Kallio K, Tsien RY, Boxer SG, Remington SJ: **Crystal structure and photodynamic behavior of the blue emission variant Y66H/Y145F of green fluorescent protein.** *Biochemistry* **1997**, 36: 9759-9765.

[3] Hakim NH, Kounishi T, Alam AH, Tsukahara T, Suzuki H: **Alternative splicing of Mef2c promoted by Fox-1 during neural differentiation in P19 cells**. *Genes Cells* **2010**, 15: 255–267.

[4] Using Michael Zucker's mfold [5] Web server (http://www.bioinfo.rpi.edu/applications/mfold.)

[5] Zuker M: **Mfold web server for nucleic acid folding and hybridization prediction**. *Nucleic Acids Research* **2003**, 31(13), 3406-3415.

CHAPTER V: FINAL DISSCUSSION

RNA editing is post-transcriptional process to change one or more nucleotides in the sequences of RNA. This process naturally makes the diversity of protein and various phenotypes. RNA editing has divided to five types, and the A-to-I editing and C-to-U editing were two common types in human. RNA editing could reprogram of nucleotide, therefore many attempts were carried out to control or mimic the RNA editing. One of these approaches was the enzyme site-directed RNA editing. The enzyme site-directed RNA editing was almost mimicked the A-to-I editing. In the first step, the ADAD enzyme was engineered by replacing the dsRNA to guide RNA. The targets are the mutated RNAs, having premature termination codons (UAA, UAG, UGA), and try to reprogram to tryptophan (UGG). Consequently, protein function could be partly and totally restored.

C-to-U editing has very promising application for treatment of diseases which were caused by T>C or G>A mutations. Because the C-to-U editing was catalyzed by a multicomponent protein complex (editsome) rather than single protein in A-to-I editing, it is very difficult to construct the recombinant enzyme. We recently reported a strategy for site-directed non-enzymatic chemical RNA editing that allows application of C-to-U editing. By reprogramming guanosine to adenosine, our method has a lot of potential to partly repair genetic disease phenotypes. The recombinant enzyme was not used therefore our method is simple, not expensive and non-toxic. Our strategy was firstly reported by Prof. Fujimoto and colleagues. In their protocol, template-directed DNA photoligation was

mediated by artificial oligonucleotides, a short single strand 20-mer target was used and the C-to-U substitution was highly efficient and sequence-specific without any side-reactions *in vitro*. In our works, this method was studied and developed to apply for long single strand DNA target and full-length RNA target.

In chapter 2, a mitochondrial DNA T8993C mutation of Leigh syndrome patient was used as model. We carried out converted C8993U by artificial site-directed chemical RNA editing. We designed and synthesized 5 ^{CV}U-containing ODNs, and the experimental results revealed that ODN2 could convert C to U most effectively among examined 5 ^{CV}U-ODNs. We succeeded a sequence-specific photochemical base substitution toward ss72-nt, ss731-nt, RNA823-nt and total RNA from patient's cells used as targets. We found that almost 10% of RNA was successfully deaminated *in vitro*. Better results were observed when the heat- treatment was performed at 37 °C instead of 90 °C by using RNA as a target. It is known that RNA is strongly degraded in higher temperature. The result might be caused by stabilization of RNA in lower temperature.

In chapter 3, in order to apply to further *in vivo* study, we changed model to BFP. Blue fluorescent protein (BFP), a derivate of green fluorescent protein (GFP), differs from GFP by a single nucleotide; a C-to-T change at position 199 transforms the BFP gene into the GFP gene. We successfully performed site-directed photochemical base substitution in synthetic ss100-nt and *in vitro*-synthesized full-length BFP mRNA targets. ODNc exhibited most effective C199U transition under physiological temperature among the three tested

^{CV}U-containing ODNs. ODNc contains longer hairpin sequences than do ODNa and ODNb; this appears to work effectively because long sequences increase the stability of ODNs. The C199U transition was more effective in the case of ODNb than in the case of ODNa because the comparatively longer complementary sequence of ODNb will bind more strongly to the target. The relationship between ODN sequences and deamination efficiency is crucial and need further study. We determined that approximate 10% of the full-length mRNA was deaminated in *in vitro* deamination under physiological temperature.

In chapter 4, the structure and sequence of ^{CV}U-containing ODNs are key features of ODNs on its biological functions. To investigate the relationship between the ^{CV}U sequences and deamination efficiency, a series of oligodeoxynucleotides (ODNs) were designed and subjected to site-directed, non-enzymatic editing. From these experimental results, we showed that there are strong relationship between the deamination efficiency, and the sequence complementary length and hairpin loop length. Our investigation showed that the optimal deamination efficiency was achieved with ODNs having a sequence complementary length slightly more than 14nt and a hairpin length of 9nt. In order to confirm our conclusions on the optimum conditions for the ODNs, we designed, synthesized, and surveyed a new ODN with these conditions, i.e., an ODN has a sequence complementary length of 15nt and a hairpin length of 9nt (ODN8). The results were shown that ODN8 has best deamination efficiency comparing to other ODNs. And this study has

important significance to design the suitable, optimum oligodeoxynucleotides (ODNs) for treatment of every T>C or G>A caused diseases by using site-directed transition approach.

In summary, we successfully performed site-directed photochemical base substitution to restore the mutated mRNA to a “healthy RNA” under physiological temperature by using photochemical base substitution. We believe that the site-directed photochemical deamination technology could serve as a new approach for genetic restoration. Here, we designed and studied site-directed chemical deamination for genetic restoration *in vitro*. *In vivo* studies that include cultured cells and model animals will be conducted in the near future because of the requirement of relatively more complex technology.

LIST OF PUBLICATIONS

JOURNALS

1. Vu TL, Ooka Y, Alam S, Suzuki H, Fujimoto K, and Tsukahara T: **Chemical RNA editing as a possibility novel therapy for genetic disorders**. *IJAC* **2012**, 2(6): 237-241.

2. Suzuki H, Takeuchi M, Sugiyama A, Alam AHMK, Vu TL, Sekiyama Y, Dam HC, Ohki S, and Tsukahara T: **Alternative splicing produces structural and functional changes in CUGBP2**. *BMC Biochemistry* **2012**, 13:6.

3. Vu TL, Nguyen TKT, Alam S, Sakamoto T, Fujimoto K, Suzuki H and Tsukahara T: **Change from Blue Fluorescent Protein to Green Fluorescent protein by Chemical RNA Editing as Novel Strategy in Genetic Restoration**. In press. *Chemical Biology and Drug Design*.

4. Vu TL, Nguyen TKT, Md Thoufic AA, Suzuki H and Tsukahara T: **The Relationship between Structures and Deamination Efficiency of Carboxyvinyldeoxyuridine ODNs on Chemical RNA Editing for Genetic Restoration**. In preparation.

ACKNOWLEDGEMENTS

First of all, I would like to express my deep thanks towards my supervisor, Prof. Dr. Toshifumi Tsukahara Sensei for all his good advices, encouragement, extreme patience, whole-hearted guidance and also providing me with useful ideas and suggestions especially in the process of completing my master and doctoral programs. And I would like to take this opportunity to send my sincerest gratitude and thanks to my beloved parents with their forever love and unfailing supports, help me to achieve success in all my life.

Next, I would like to express my sincerest gratitude and thanks to my husband and my sons for being supportive. Thank to my beloved husband for his motivation, supports and assistance.

I would like to extend my thanks and appreciation to Vietnamese government scholarship and GRP scholarship for providing me with financial supports to complete my master and doctoral programs.

I would like to extend my thanks and appreciation to Prof. Dr. Masayuki Yamaguchi and Associate Prof. Dr. Dam Hieu Chi for their guidance in my subtheme researches.

I would like to extend my thanks and appreciation to Prof. Dr. Takahiro Hohsaka for teaching me about fluorescent data processing.

I would like to extend my thanks and appreciation to my sub supervisor, Prof. Dr. Shin-ya Ohki for useful experimental machines and supports.

I would like to extend my thanks and appreciation to Assistant Prof. Dr. Hitoshi Suzuki for guiding me with useful experimental techniques.

To the judging committee; I would like to thank the internal panels; Professor Dr. Toshifumi Tsukahara, Professor Dr. Shin-ya Ohki, Professor Dr. Takahiro Hohsaka and Associated Professor Dr. Hidekazu Tsutsui of School of Materials Science, JAIST, as well as the external panel, Dr. Shinichi Takeda from NCNP National Institute of Neuroscience; for your evaluation, reviews, suggestions and advices throughout the process of completing my doctoral dissertation.

I would like to extend my thanks and appreciation to all Tsukahara Sensei Lab members, especially my seniors, Dr. AHM Khurshid Alam, Dr. Shafiul Alam, and Dr. Nor Hakima Binti AB Hakim for their assistant and help throughout completing my project as well as present lab members Mr. Thoufic Anam Azard.

I would like to extend my thanks and appreciation to my friends for their assistant and help throughout completing my project.